University of Szeged

Faculty of Pharmacy

Department of Medical Chemistry

BOTTOM-UP DESIGN OF FOLDAMERS FOR PROTEIN SURFACE RECOGNITION

Ph. D. Thesis

Éva Karolina Bartus

Supervisor:

Prof. Dr. Tamás Martinek

2019

Table of content

List of publications and lectures

Full papers related to the thesis

I. É. Bartus, G. Olajos, I. Schuster, Zs. Bozsó, M. A. Deli, Sz.Veszelka, F. R. Walter, Zs. Datki, Zs. Szakonyi, T. A. Martinek, L. Fülöp (2018). Structural Optimization of Foldamer-Dendrimer Conjugates as Multivalent Agents against the Toxic Effects of Amyloid Beta Oligomers. *Molecules,* 23(10), 2523.

IF: 3.098

II. G. Olajos, É. Bartus, I. Schuster, G. Lautner, R. E. Gyurcsányi, T. Szögi, L. Fülöp, T. A. Martinek (2017). Multivalent foldamer-based affinity assay for selective recognition of Aβ oligomers. *Analytica chimica acta*, **960**, 131-137.
IF: 5.123

III. É. Bartus, Zs. Hegedüs, E. Wéber, B. Csipak, G. Szakony, T. A. Martinek (2017). De Novo Modular Development of a Foldameric Protein–Protein Interaction Inhibitor for Separate Hot Spots: A Dynamic Covalent Assembly Approach. *ChemistryOpen*, **6** (2), 236-241.
IF: 2.801

Other full papers

IV. A. Hetényi, L. Németh, E. Wéber, G. Szakonyi, Z. Winter, K. Jósvay, É. Bartus, Z. Oláh, T. A. Martinek. (2016). Competitive inhibition of TRPV1–calmodulin interaction by vanilloids. *FEBS letters* **590**(16): 2768-2775.
IF: 3.623

Scientific lectures related to the thesis

1. Bartus É., Hegedüs Zs., Wéber E., Csipak B., Szakonyi G., Martinek T.
   Célfehérje által vezérelt ligandum tervezés rendezett fragmensek segítségével - Affinitás-növelés
   MTA Peptidkémiai Munkabizottság Tudományos Ülése
   Balatonszemes, 2016. május 30- június 1.

2. Bartus É., Hegedüs Zs., Wéber E., Csipak B., Szakonyi G., Martinek T.
   Célfehérje által vezérelt ligandum tervezés rendezett fragmensek segítségével
   Magyar Tudomány Ünnepe Előadóülés
   Szeged, 2016. november 8.

3. É. Bartus, Zs. Hegedüs, E. Wéber, B. Csipak, G. Szakonyi, T.A.Martinek
   Target directed synthesis of foldameric protein–protein interaction inhibitors
   Poster presentation
   Blue Danube Symposium on Heterocyclic Chemistry Conference
   Linz, August 30-September 2, 2017.

4. Bartus É., Mag B, Csipak B., Ecsédi P. Nyitray L. Martinek T. Proteinek felismerési mintázata a foldamer térben
   MTA Peptidkémiai Munkabizottság Tudományos Ülése
   Balatonszemes, 2018. május 28-30.

Abbrevations

ABHC: (1*S*,2*S*,3*S*,5*R*)-3-amino-6,6-dimethylbicyclo[3.1.1]heptane-2-carboxylic acid

ACHC: (1*S*,2*S*)-2-aminocyclohexanecarboxylic acid

AD: Alzheimer's disease

APP: Amyloid precursor protein

AUC: area under curve

Aβ40: β-amyloid 1-40

Aβ42: β-amyloid 1-42

Bcl-2: B-cell lymphoma-2

BSA: bovine serum albumin

CaM: calmodulin

DBU: 1,8-diazabicycloundec-7-ene

DCC: dynamic combinatorial chemistry

DCL: dynamic combinatorial library

DCM: dichloromethane

DIEA: *N*,*N*-diisopropylethylamine

DMF: *N*,*N*-dimethylformamide

DTT: 1,4-dithiotreitol

EC_{50}: half maximal effective concentration

ELISA: enzyme-linked immunosorbent assay

ESI-MS: electrospary ionization mass spectrometry

Fmoc: fluorenylmethyloxycarbonyl

G0-PAMAM: tetravalent-zero generation poly(amidoamine)

GLP-1: glucagon-like peptide-1

GSH: reduced glutathion

GSSG: oxidized glutathion

HATU: 1-[bis(dimethylamino)methylene]-1*H*-1,2,3-triazolo[4,5-*b*]-pyridinium-3-oxid hexafluorophosphate

HBS: hydrogen bond surrogate

HEPES: 4-(2-hydroxyethyl)-1-piperazineethanesulfonic acid

HMW: high molecular weight

HRP: horseradish peroxidase

HTS: high-throughput screening

IL2: interleukin 2

ITC: isothermal titration calorimetry

LMW: low molecular weight

MDM2: mouse double minute 2

MPA: 3-maleimidopropionic acid

PBS: phosphate buffer saline

PPI: protein–protein interaction

SPPS: solid-phase peptide synthesis

SRM: single reaction monitoring

tBu: *terc*-butyl

TFA: trifluoroacetic acid

TIS: triisopropylsilane

TMB: 3,3',5,5'-tetramethylbenzidine

TRPV1: transient receptor potential vanilloid 1

VEGF: vascular endothelial growth factor

VEGFR1: vascular endothelial growth factor receptor-1

1. Introduction and aims

Molecular recognition events are controlled by specific noncovalent interactions and they play key role in almost all biological processes[1-3]. Intermolecular contacts are affected by many different factors including shape and electrostatic complementarity of the molecular surfaces[4, 5]. Focusing on protein–protein complexes, the free energy of the binding is directly related to the buried mostly flat surface area, which lacks deep binding pockets shielded from water. These interactions are therefore coined "undruggable" for a small-molecule drug candidate[6, 7]. In order to modulate the function of such protein complexes, extended molecular surface mimetics are required with a specific arrangement of the hot-spot residues[8-11]. This can be achieved by synthesizing rigid scaffolds via introducing cyclic constraints into the molecules; thus, the interacting surface is a direct product of the chemical synthesis[12, 13]. The well-defined shape of the molecule can be created in a subsequent stage through a folding procedure depending on the solution conditions and interacting partners. Typically, biopolymers and their structural mimetics can self-organize into these kinds of hierarchical structures. In terms of molecular recognition, foldamers, i.e., non-natural oligomers with distinct conformational preferences, are interesting, due to their ability to mimic structure and functions of biopolymers[14-16]. Predictable three-dimensional structures can be generated from monomeric modules leading to large exposed surface patches, which make foldamers attractive tools for high-affinity, specific recognition of protein interfaces[17, 18]. Although ribosomal incorporation of foldameric building blocks has been achieved in special cases[19], foldamers are fundamentally evolution-free chemical entities. *De novo* or bottom-up design strategies are therefore particularly difficult for foldamer sequences in cases, where limited structural information is available about the target surface.

Our main goal was to design foldameric binders for the recognition of difficult protein target surfaces[6] by applying bottom-up design approaches. One of our molecular targets was the soluble β-amyloid oligomer[20-23]. Its level in cerebrospinal fluid correlates with the cognitive impairment in Alzheimer's disease, which makes it an attractive biomarker for monitoring the progression of the disorder[24, 25]. Application of the foldamer methodology and the fragment-based approach resulted in the development of high-affinity interacting partner for β-amyloid. Therefore, by exploiting this interaction, the aim was to optimize a sandwich-type affinity assay using multivalent foldamer conjugate as a capture antibody mimetic. In order to develop a specific and selective assay, structural optimization of the capture molecule and increasing the efficiency of the detection system were necessary.

As another target, a model protein calmodulin having two separate hot-spot pockets[26, 27] was chosen for modular bottom-up design of a foldameric inhibitor. In order to find weakly interacting partners of the protein, a surface-patch mimetic library containing short foldameric fragments was screened and the simultaneous optimization of the two binding hot spot fragments was achieved by ligating the hits via dynamic combinatorial chemistry[28].

2. Literature background

2.1. Characterization of protein interfaces

Molecular recognition is fundamentally determined by the free energy of binding[1, 2]. Investigation of host–guest complexation provides deeper insight into protein functions and elementary processes of biological systems. Although protein–protein interactions (PPIs) have promising therapeutic potential[29-31], protein surfaces are difficult to recognize with synthetic molecules[11]. The main reason is that protein interfaces, through which the direct physical contact occurs, are usually large and shaped irregularly requiring extended molecules for selective, high-affinity interaction[32]. There are a number of factors, which characterize these seemingly featureless surfaces such as electronic properties (charge, polarity, polarisability, van der Waals attraction and repulsion), size, shape, number, and arrangement of the binding sites on the interfaces[5].

2.1.1. Buried surface area and hot-spot residues

The interaction interfaces have relatively large complementary surface areas, which vary in the range 1500–3000 Å^2[4, 33]. Compared with the average contact area between a small ligand and a receptor (300–1000 Å^2), the former values are considerably larger. Consequently, a high-molecular weight PPI inhibitor is required to meet challenges associated with the free-energy contributions scattered over the extended contact surfaces. Hydrophobic interaction is the main driving force for PPIs[34], and electrostatic complementarity interactions, i.e., hydrogen bonds and salt bridges also stabilize protein complexes[35, 36]. Interfaces are fundamentally modular and the key stabilizing interactions are not homogeneously distributed. Residue mutations to Ala causing a significant change in the binding free energy (at least 2 kcal mol^{-1}) are defined as hot-spot residues[10, 37], and these contribute dominantly to the stability of the protein–protein complexes. These special modules are structurally conserved and alanine scanning studies indicate distinctive amino acid compositions[8, 37-39]. If the total interaction surface is under 2000 Å^2, it is usually composed of a single patch, whereas larger contact surfaces are created by separate hot-spot patches surrounded by solvent-exposed regions leading to a discontinuous epitope[38].

2.1.2. Classification of protein–protein interactions

On the basis of common structural elements and the modes of interaction, protein–protein complexes can be classified into four main categories[4], which fundamentally define the druggability of the interactions[6, 11] (Figure 1). „Tight and narrow" interactions are the most

similar to the classical receptor–ligand model and, therefore, these PPIs have proven to be the most amenable to inhibition. This kind of interaction occurs, for example, between interleukin 2 (IL-2) and IL-2α receptor[40], mouse double minute 2 (MDM2) and p53 tumor suppressor protein[41], and between the anti-apoptotic Bcl-2 family members and BH3 domain of pro-apoptotic BAK/BAX[42]. There is a rich literature with respect to successful development of small-molecule PPI inhibitors. In these cases, the hot-spot residues usually group within a tightly packed cluster, typically in a binding cleft for α-helix recognition on the surface of a globular protein[6, 43]. In contrast, PPIs within category „Loose and Narrow" are formed through relatively small contact areas, and the shallow binding pocket allows just a weak interaction making them difficult to target. They are usually transient complexes and there are only a few examples of their successful inhibition[44, 45]. "Loose and Wide" interactions are the most extremist cases of the PPIs, characterized by large interacting surfaces and micromolar affinities. The Ras/SOS (Son of Sevenless) complex is one of the few examples of PPIs belonging to this category and it was successfully inhibited with small-molecule ligands[46]. The most challenging task is probably the disruption of globular protein complexes belonging to category „Tight and Wide". In these PPIs, the recognition of a relatively large and flat surface is required[47] with frequent involvement of convoluted or discontinuous interaction surfaces (Figure 1). The most potent inhibitors are extended molecular surface mimetics that can provide specific arrangement of the desired hot-spot residues.

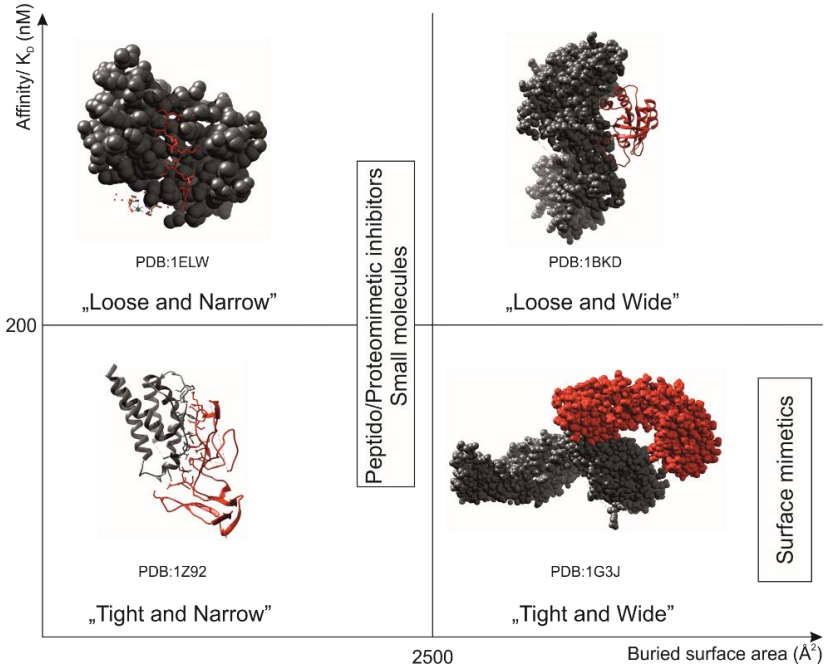

Figure 1. Classification of protein–protein interactions (PPIs) on the basis of the buried surface area and the binding affinity. Narrow interacting surfaces require small-molecule inhibitors, while protein complexes rely on wide contact areas usually requiring extended surface mimetics.

2.2. Targeting protein recognition surfaces

Targeting a large solvent-exposed protein interface requires inhibitors with comparable surface area, which can compete successfully for separate hot-spot binding sites. In inhibitor design, precise projection of the multiple anchor points is crucial for high-affinity binding[32, 48]. Beside antibodies, which are still the gold standards for high-affinity recognition, there are two main strategies to create distinct molecular shapes: multivalent presentation of recognition domains on a rigid supramolecular scaffold or formation of a well-defined molecular surface in a subsequent folding process.

2.2.1. Antibody mimetics

Despite the poor pharmacokinetic properties, immunogenicity, and costly time-consuming production, antibodies are still the most efficient tools for selective, high-affinity molecular recognition. To overcome their limitations, there is a growing interest in artificial antibody mimetics. They are functional mimetics of antibodies having tailored characteristics but retained low nanomolar binding affinity toward antigens[49, 50]. On the basis of the originating proteins, we can distinguish different types of these engineered scaffolds, such as affibodies, adnectins, affimers, anticalins, fynomers, knottins, DARPins, etc. Some of them already have remarkable importance as diagnostics and in therapeutic applications[51-53].

2.2.2. Protein surface mimetics

An obvious solution to extend the surface of a small molecule is linking together multiple copies, where multivalency increases the binding affinity of a given ligand. Positioning the multiple recognition elements on a suitable rigid scaffold results in multivalent non-covalent contacts over a large area of protein surface. Rigid scaffolds like anthracenes, calixarenes, porphyrins, cyclodextrins, and resorcinarenes ensure direct coordinative interactions and selective binding of higher affinity can be achieved[54-57].

2.2.3. Peptide-based protein–protein interaction inhibitors

Peptides, because of their low conformational and proteolytic stability, are normally not preferred as drug candidates. Nevertheless, they are promising starting materials to develop PPI inhibitors. Increasing the stability of the active conformation could increase the binding affinity to the target and, at the same time, decrease the possibility of degradation. These are mainly secondary structure mimetics, where two strategies available for their production are the rigidification of the molecule via cyclization and the modification of the backbone to increase protease resistance (Figure 2)[13, 48].

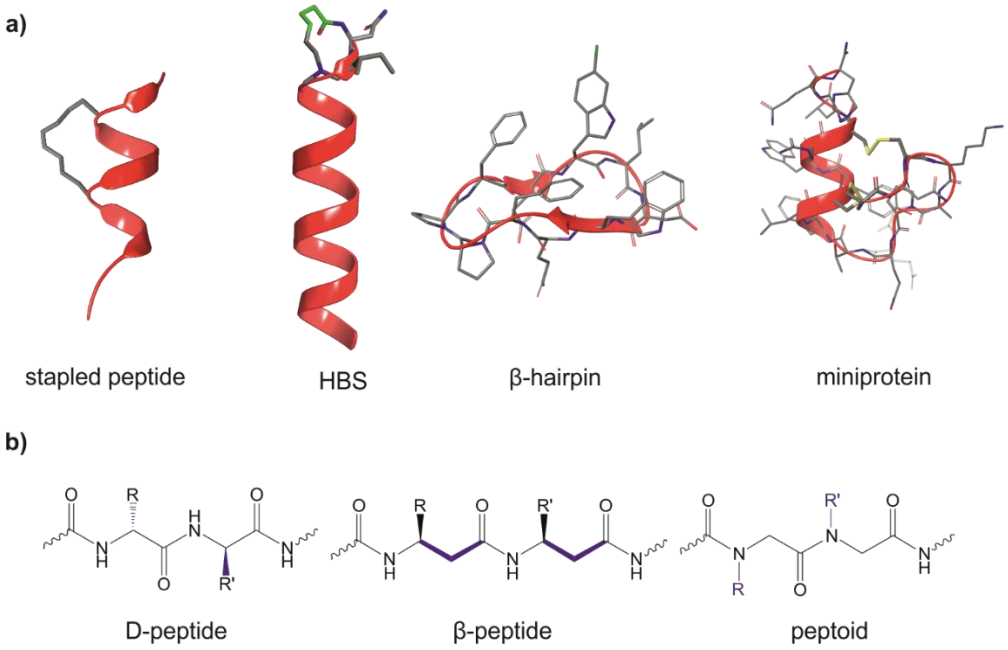

Figure 2. Structural modification possibilities to create peptide-based inhibitors with improved conformational and proteolytic stability: **a)** stapled peptide resulting from cyclization (pdb: 2YJA), HBS (hydrogen bond surrogate, pdb: 4MZL), β-hairpin (pdb: 2AXI), and miniprotein (pdb: 3IUX); **b)** backbone modifications.

Cyclopeptides can mimic native protein structures while exhibiting enhanced metabolic stability[12]. The structural preorganization limits their conformational flexibility and reduces the entropic cost of binding. Cyclization can be performed by covalent coupling of the C- and the N-terminal end of the peptide sequence (head-to-tail) to stabilize the active conformation of the native ligand[58]. Joining side chains by covalent bonds, which are in spatial proximity in the desired conformation, results in stapled peptides (Figure 2a). Usually, *i*, *i*+4 or *i*, *i*+7 hydrocarbon staples are formed to stabilize α-helical structure[59, 60]. Very often, however, these crosslinks cause additional hydrophobic interactions and lower solubility, which alter both the recognition properties and the selectivity of the stapled form[61]. The hydrogen bond surrogate (HBS) strategy is also based on the formation of a peptide macrocycle, where an *i* to *i*+4 backbone hydrogen bond is replaced by a carbon–carbon bond[62, 63] (Figure 2a). The crosslinker of an HBS ligand is less exposed to the enviroment relative to the stapled helix crosslinks, and the side-chain functionality is retained. Protein-binding peptidic epitopes can be incorporated into a semi-rigid macrocycle with a turn-inducing unit (Figure 2a). Such β-hairpin peptidomimetics are composed of two consecutive H-bonded antiparallel β-strands, where the size of the hairpin loop is a variable parameter[64]. Another interesting scaffold to graft the identified binding epitopes are miniproteins, namely, oligopeptides with three-dimensional structure stabilized by disulfide moiety[65] (Figure 2a). The well-defined, stable folded structure

ensures the specific arrangement of the side chains of the epitope sequence and stabilizes the linear peptide binders, which can improve the binding affinity of the peptidic ligands.

Backbone modified peptidomimetics with improved proteolytic and conformational stability are other promising alternatives to peptidic analogs. The major possibilities are i) the use of D-analogs of the natural L-amino acids, ii) substitution of some or all amino acids to β-homologs, iii) repositioning the proteinogenic side chains to the peptide bond nitrogen atom by using peptoid as a scaffold (Figure 2b). Replacement of the L-amino acids to D-amino acids is a well-known strategy to develop peptide-based bioactive compounds, that significantly reduce the possibility of proteolytic degradation[66, 67]. Although retro-inverso isomerization allows similar side chain topology as its parent molecule with inverted amide peptide bonds, sometimes it works poorly in molecular mimicry of biologically active helices[68]. Despite the similar side-chain topology, it is not equivalent with the L-analogs at the secondary structure level, and the binding mode for the D-variant fragments usually differs from the native ligand. β-Peptides are oligomers containing β-amino acids exclusively or in combination with α-amino acids. As they have a high tendency to form stable conformations in solution, these molecules are referred to as β-peptide foldamers and they are discussed in details in the next section. Peptoids are N-substituted oligo-glycines belonging to the family of peptidomimetic foldamers due to their structural similarities[69, 70]. The nitrogen of the peptide bond contains the side chain and, therefore, it loses the ability to serve as a hydrogen donor and, therefore, peptoids require fundamentally different stabilization of the secodary structure. The lack of stabilizing backbone H-bonds makes the peptoids highly flexible and, therefore, the *de novo* design of well-defined secondary structures is challenging. Nevertheless, they are still attractive scaffolds for biomedical applications[69, 71].

2.3. β-Peptide foldamers

β-Peptides are the most extensively studied subset of foldamers, i.e., they are self-organizing synthetic oligomers with high propensity to form well-defined structural elements[72, 73]. The β-peptide foldamers are programmable structural and functional mimetics of biopolymers, which makes them promising alternatives for biopharmaceuticals[16]. Introducing unnatural β-amino acids into the α-peptide backbone significantly increases the proteolytic stability of the peptide[74, 75]. Even when the chain lengths are as short as five or six residues, they are able to fold into distinct secondary structures (helices, turns, and strands) that can exhibit similar interaction surfaces to larger proteins, which is particularly advantageous for protein surface recognition[32, 48, 76].

2.3.1. Building blocks and secondary structures

The difference between β- and α-amino acids is that the former is elongated with one methylene (C_β) in the backbone. Furthermore, due to the additional substitution position and stereogenic center, the β-amino acid building blocks are characterized by higher diversity (Figure 3). Depending on the substitution pattern of the monomers we can distinguish β^2-, β^3-, and $\beta^{2,3}$-amino acids and their syntheses are performed in different ways[77]. For β^2-amino acids, the overall enantioselective Mannich reaction or Curtius degradation is applied. The β^3 building blocks are obtained by Arndt–Eistert homologation of α-amino acids[78, 79], and they are now commercially available with a few exceptions (β^3hHis, β^3hCys, β^3hSec)[80]. The $\beta^{2,3}$-amino acids are prepared from the appropriate β^3-amino acids by enolate alkylation. Both the C_α and C_β atoms can be in a cycloalkane or a heterocyclic ring, which decreases the conformational flexibility and stabilizes a given secondary structure[81]. Beside pure β- peptides, α/β-peptide foldamers can be synthesized by introducing β-amino acids into the α-peptide chain in appropriate combination (ααβ, αααβ, ααβααβ) to ensure substantial protection from degradation but retain α-helical conformation[82].

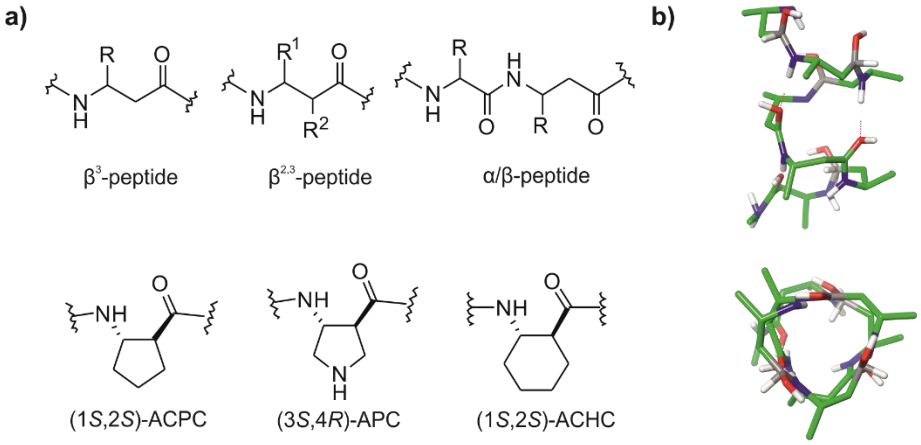

Figure 3. Structural diversity of β-peptide foldamers: **a)** monomeric modules with additional substitution position and cyclic derivatives, **b)** side and top views of a 14-helix of a pure β-peptide.

From molecular recognition point of view, the predictable structures of the β-peptides are particularly advantageous, and the diverse secondary structures give us a useful toolbox for inhibitor design. Similar to α-peptides, the secondary structures are stabilized by hydrogen bonds and the folding depends on local conformational preferences and long-range hydrophobic interactions. The β-amino acid units having specific stereochemical configuration and stereochemistry not only define the primary sequence of the peptide, but its secondary structure is also predictable from the sequence of monomers. The stereochemical pattern of the backbone encodes the folding propensity of the molecule: if the signs of the torsions flanking the amide

moiety are the same, a helical conformation will be formed whereas if they are opposite, then a strand is induced[17]. The whole palette of β-peptide secondary structures is diverse containing helices with different inner diameter, turns, and strands. Folding behaviours of these oligomers are multifactorial, and several different helix and strand conformations have been experimentally observed such as 8-, 10-, 10/12-, 12-, 14-, 14/16-, 18-, 18/20-helices, extended polar, Z6 non-polar, and alternating polar strands[83-85]. Beside the stereochemical pattern of the backbone, the folded shape of the molecule is affected by i) the chain length of the oligomer, ii) the bulkiness of the monomeric units, iii) the amount of the dihedral constraints in the sequence, and iv) solution conditions. Application of an α/β heterogeneous backbone can further increase the diversity, depending on the α/β ratio and their pattern, unique helical structures such as 14/15-, 11-, 9/10/11/12-helices can be induced[86, 87].

The predictable folding behaviour and improved proteolytic stability makes the class of foldamers a promising candidate for protein surface recognition. Several proteins have already been targeted with foldamers, such as Bcl-xL-BAK, hDM2-p53, VEGF-VEGFR1 complexes[18, 88-91], somatostatin, parathormon, and GLP-1 receptors[92-94].

2.3.2. Bottom-up design approaches for molecular recognition

The development of complex molecular building blocks having controllable morphologies and functionalities is required for the interaction with biological interfaces. While extensive knowledge of the structure of the interacting partner is needed for top-down design, bottom-up design strategies require the ability to *de novo* build-up molecules in a highly controlled manner. Top-down approaches are frequently used for foldamers and other peptidomimetics[82, 95], but limited structural information about the target or the lack of known peptidic binder makes the ligand design more challenging. Despite the fact that foldamers are able to make predictable three-dimensional structures thus providing specific arrangement of the proteinogenic side chains, there are only a few examples to create a foldameric ligand by using *de novo* bottom-up approaches.

Fragment-based methods are iterative small-to-large molecule strategies. The iterative process consists of at least two main steps: i) a fragment screening, during which weakly-binding (K_D=0.1–10 mM) low-molecular mass fragments are identified, ii) a fragment elaboration with merging, linking or growing to develop more potent compounds of larger molecular weight[96]. Although it is frequently used in small-molecule drug candidate[97], this method is not used among foldamers with some notable exceptions[98, 99].

Another versatile tool to find high-affinity protein binders is high-throughput screening (HTS) of large libraries of compounds. In larger libraries (up to 10^6) the compounds are usually simplified, not druglike molecules. However, if we increase the complexity of the members with the necessary size reduction of the library, only a small fraction of possible chemical space can be investigated. Therefore, further optimization of the hits is required in every case.

2.3.3. Dynamic combinatorial chemistry

Conventional drug discovery methods are slow and expensive, because the technology consists of iterative cycles of design–synthesis–screening. There is therefore a growing interest in using directed evolution methods for reliable optimization of protein binders[100]. When mimicking the natural evolution process *in vitro*, the synthesis and screening of large libraries occur simultaneously. Since unnatural foldamers are fundamentally evolution-free chemical entities, *in vitro* evolution methods are not applicable for the optimization of their structure, but dynamic combinatorial chemistry (DCC) can be an alternative for designing functional materials[101]. Dynamic combinatorial libraries (DCLs) rely on the reversible generation of compound mixtures under thermodynamic control, where the overall system can adapt to external stimuli such as addition of a protein template by shifting the dynamic equilibrium towards the formation of the tightly binding ligands[102, 103]. Driven by thermodynamic control, the final product distribution is formed on the basis of the position of different compounds in the free-energy landscape, which eventually causes the main limitations of the methods[104]. In DCL experiments, the template concentration and the size of the library are the most crucial parameters. To the introduction of a target protein, DCLs respond in a way to minimize the free energy of the entire system. Small, but weaker binders are preferred over larger, but strong binders, because the overall entropic penalty is usually high in the latter case. Furthermore, a large number of weak binders successfully compete with the few strong binders[105]. At high template concentration, these unwanted phenomena are even more pronounced, because the large amount of template does not restrict the number of binding sites. In this case, the overall amplification of the library members is significantly increased, which is advantageous for analysis, but the selectivity is drastically decreased[106]. Detailed calculations show that application of about 0.1 equivalent of template even in larger libraries results in a good correlation between amplification and binding[106]. Investigation of larger libraries provides higher probability of identifying the best binder, because the affinity of the detected members increases with the increasing library size[104]. Due to simple probability, the formation of homomeric library members is less preferred over that of heteromeric ones. If a homo-oligomer

is still a good binder, its amplification indirectly upregulates other library members devoid of the corresponding building block[107]. This co-amplification may further decrease the probability to find real good binders. Taking these into account, finding the best binder in this way means drawing correct conclusions from really complex response of DCLs to molecular recognition events, that requires careful design of the buliding blocks, experiments, and analyses.

2.4. Targeting β-amyloid oligomers

2.4.1. Alzheimer's disease and β-amyloid peptide

Alzheimer's disease (AD) is one of the most common neurodegenerative disorder[108]. Although the cause of the disease is poorly understood, its progression is in close relation to β-amyloid peptides, the cleavage products of amyloid precursor protein (APP)[25, 109]. The primary products of secretases are β-amyloid peptides with lengths of 40 and 42 amino acids (Aβ40 and Aβ42). Studies confirmed that the longer-sequence Aβ42 shows higher aggregation propensity[110], and it is more toxic to neuronal cells. It has also been shown previously, that the mostly disordered Aβ42 monomer has a neuroprotective effect on neuronal cell culture[111], but the peptide can rapidly form structured monomer (β-hairpin) and associates to create oligomers, protofibrils, and fibrils depending on the conditions (peptide concentration, pH, temperature, salt concentration, etc.). Despite the fact that physiological effects of these associated species are intensely studied, their direct connections to different states and the progression of AD are still not fully understood. Several pieces of evidence prove that soluble Aβ42 oligomers are the most neurotoxic assemblies. They drive the degenerative pathology of AD, and their amount in the cerebrospinal fluid shows correlation with cognitive decline[20, 112]. Therefore, the Aβ42 oligomer can serve not only as a therapeutic target but also as a potential biomarker to monitor the progression of the disease. The structure of the amyloid fibril is now well-characterized[113] in contrast to neurotoxic Aβ42 oligomers. The structural polymorphism and sample heterogenity make the high-resolution structure of the oligomer difficult to study[114]. In the aggregation pathway of amyloid, monomers can form oligomers of low and high molecular weight (LMW and HMW). Both oligomers are disc-shaped with diameters of about 10–15 nm[21, 115]. Within the oligomer, the N-terminal ends (residues 1–13) of the monomeric units are disordered with high flexiblity. The middle part of the peptide (residues 14–23) is the self-recognition region, which is responsible for the lateral association of the unstructured oligomers and β-sheet formation. The C-terminal ends create the hydrophobic core of the oligomer and mediate fibril formation by stabilizing the cross β-sheet structure. The solvent-exposed

hydrophobic patch in the middle part of the sequence $K^{16}LVFFAE^{22}$ (Figure 4) is identified as an intermolecular contact during oligomerization and most of the small-molecule and peptidic inhibitors target this part of the Aβ aggregates[116].

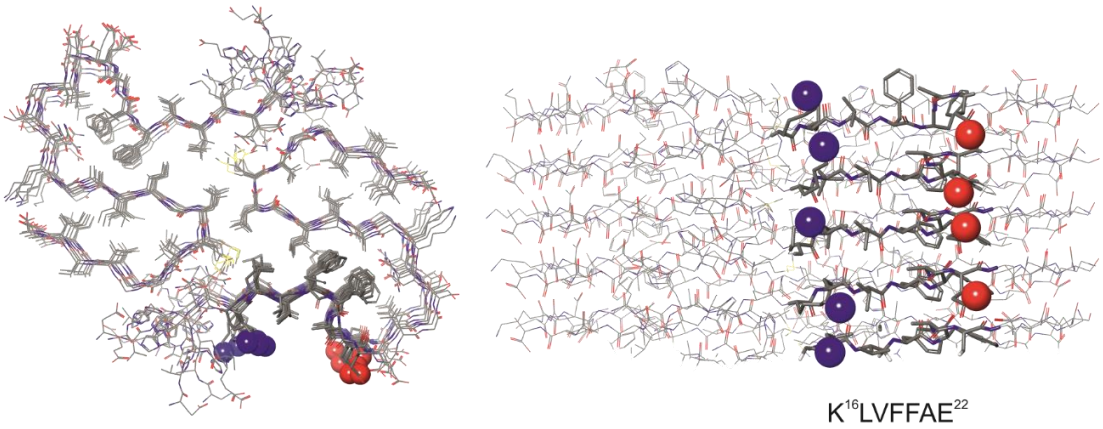

Figure 4. Top and side view of the high-resolution structure of monomorphic Aβ fibrils[117] (pdb: 5KK3). The solvent-exposed $K^{16}LVFFAE^{22}$ sequence is highlighted.

2.4.2. Sensitive detection of β-amyloid

On the basis of strong belief in the amyloid cascade hypothesis[109], many AD drug developments focus on targeting the production, fibrillation, and clearance of Aβ. The possible reason for Aβ-related treatment strategies failing at clinical studies is that the pathogenesis of AD is multifactorial. Consequently, for effective therapy, early detection before the start of the irreversible neurodegeneative processes would be essential[118]. Sensitive quantification of the potential biomarker Aβ oligomer may be suitable for early diagnosis of the disorder and for monitoring the effect of different anti-AD treatments. It is especially important in those stages, where the asymptomatic nature of the disease makes the diagnosis difficult. Current diagnostic methods are mostly based on imaging of Alzhemer's disease plaques in the brain in the later stage of the disorder[119]. In parallel, many strategies based on nanotechnology and biotechnology have been published for reliable detection of soluble Aβ aggregates (Table 1). The detection methods are mostly relied on high-affinity interactions between specific antibodies (capture elements) and different types of Aβ associates with very impressive picomolar limit of detection.

Table 1. Summary of strategies for early detection of AD.

Capture elements	**Targets**	**Application**	**Limit of detection***
mAb158, monoclonal Ab	Aβ42 protofibrils in CSF	sandwich ELISA[120]	1 pmol/L
BAN50, N-terminal (1–16) specific monoclonal Ab	HMW oligomers of Aβ42 in CSF	sandwich ELISA[121]	10 pmol/L
mAb4G8, sequence specific monoclonal Ab and fluorescence labeled mAb6E10	different Aβ42 aggregates in CSF	surface FIDA[122, 123]	nd
ASR1, hexamer peptoid conjugated to bead	Aβ 40/42 oligomers in CSF	MPA; Capping Aβ oligomers prior to ELISA detection[124]	1 pmol/L**
MMPs and oligonucleotide-modified Au NPs functionalized by Abs	ADDL in CSF	Bio- barcode assay[125]	0.0001 pmol/L
Silver NPs functionalized with anti-ADDL Ab	ADDL in CSF	LSPR nanosensor[126]	<10 pmol/L
mAb158, monoclonal Ab	Aβ42 protofibrils in CSF	SP-PLA[127]	0.01 pmol/L***
PrP^C immobilized on gold electrode, ALP conjugated PrP^C	soluble Aβ42 oligomer	ALP-based biosensor supplemented with ECC redox cycling[128]	3 pmol/L
Fluorescent labeled sequence specific Abs (6E10- 4G8)	soluble Aβ42 oligomer	FRET-based flow cytometric analysis[129, 130]	<1 pmol/L
A11 and OC conformation specific Abs on the surface of a silver electrode	soluble Aβ42 oligomer	EIS[131]	nd

Ab: antibody, ELISA: enzyme-linked immunosorbent assay, HMW: high molecular weight, MPA: Misfolded Protein Assay, FIDA: fluorescence intensity distribution analysis, MMP: magnetic microparticle, NP: nanoparticle, ADDL: amyloid beta-derived diffusible ligands, LSPR: localized surface plasmon resonance, SP-PLA: solid-phase proximity ligation assay, PrP^C: cellular prion protein (95–110), ALP: alkaline phosphatase; ECC: "outersphere to inner-sphere" electrochemical–chemical–chemical, FRET: fluorescence resonance energy transfer, EIS: electrochemical impedance spectroscopy
*relative to monomer concentration
** defined as 80 fM oligomer, where the average composition of one oligomer is 12 monomers
*** expressed in 0.04 pg mL^{-1}, regarding the MW of Aβ is 4.5kDa

3. Experimental methods

3.1. Synthesis and purification of peptides and conjugates

Peptides and maleimido-functionalized oligo-L-lysin-dendron scaffolds were synthesized manually by SPPS, according to the Fmoc/tBu strategy using Tentagel R RAM resin (capacity: 0.19 mmol g^{-1}) and Rink Amide AM resin (0.30 mmol g^{-1}). The Fmoc-protecting groups were removed by using 2% piperidine and 2% 1,8-diazabicycloundec-7-ene (DBU) in *N*,*N*-dimethylformamide (DMF) (5+15 minutes). Washing procedures were carried out with DMF, dichloromethane (DCM), and methanol. Peptide chain elongation was done by activating a three-fold excess of *N*-Fmoc protected amino acids with 1-[bis(dimethylamino)methylene]-1*H*-1,2,3-triazolo[4,5-*b*]-pyridinium-3-oxide hexafluorophosphate (HATU)/*N*,*N*-diisopropylethylamine (DIEA) in DMF for 3 hours. Efficiency of the coupling steps was monitored with the Kaiser test. The peptides were cleaved from the resin with a mixture of trifluoroacetic acid (TFA)/H_2O/1,4-dithiotreitol (DTT)/triisopropylsilane (TIS) (90:5:2.5:2.5) at room temperature for 3 hours. Coupling of 3-maleimidopropionic acid (MPA) to the N-terminal of the lysine dendrons was also carried out on the solid support and peptides were cleaved from the resin with a cleavage mixture of TFA/H_2O/TIS (92/5/3). TFA was evaporated and the peptide was precipitated in dried diethyl ether. The resulting free peptide precipitate was filtered off, dissolved in 10% aqueous acetic acid or in the mixture of acetonitrile/H_2O, and lyophilized.

Maleimide-thiol ligation. The purified and lyophilized maleimido-functionalized scaffolds were dissolved in 50 mM phosphate buffer (pH = 7.0) and added dropwise to the solution of 1.3 × N equivalent of peptide-thiol dissolved in the same buffer under constant stirring (N is the number of arms of the conjugate). The reaction mixture was stirred overnight at room temperature and then injected directly onto a semi-preparative reverse-phase (RP) HPLC column and for purification.

Synthesis of the foldamer fragment libraries. For the synthesis of foldamer libraries a CEM Liberty 1 microwave peptide synthesizer was used with the amino acids added manually. Rink Amide PS resin was used for solid support and HATU as a coupling reagent. (1*S*,2*S*)-Fmoc-2-aminocyclohexane carboxylic acid [Fmoc-(1*S*,2*S*)-ACHC] was applied in an excess of 3 equivalents at 75 °C for 30 minutes. β^3-Amino acid mixtures were double coupled using 0.8 equivalents at 75 °C for 45 minutes. 16 different β^3-amino acids were coupled in position 5 of the sequence and 4 different amino acids in the position 4, which yielded 64 different components in each sublibrary. Deprotection was carried out in a solvent mixture of 2%

piperidine and 2% DBU in DMF for 10 minutes at 75 °C. The foldamer mixture was cleaved by 90% TFA, 5% DTT, 5% water, then TFA was evaporated and the resin washed with acetic acid and water. Finally, the product mixture was lyophilized.

Purification. Peptides and conjugates – based on the amount of the crude product – were purified on a semi-preparative (250 × 10.00 mm) or on a preparative (250 × 21.2 mm) RP-HPLC column. According to the hydrophobicity and the size of the molecules, Phenomenex Luna (particle size: 10 μm, pore size:100 Å) C18 or Jupiter (particle size: 10 μm, pore size: 300 Å) C4 or C18 was used with the appropriate gradient elution using the following eluents: (A) 0.1% TFA in water and (B) 0.1% TFA in ACN/water (80/20). Peptide purity, confirmed by analitical RP-HPLC and ESI-MS measurements, was above 95% for all compounds. The foldamer libraries were purified by using a steep gradient (0–90% during 90 minutes with the flow rate: 4 mL min^{-1}), then fractions were analyzed by MS and each fraction that contained library members was pooled together. Library components were identified by HPLC-MS based on molecular weight and retention time estimated by hydrophobic properties of the peptides. Purity analysis was based on quantification of the total library members and impurities by integration of the HPLC-MS chromatograms.

3.2. Preparation of β-amyloid samples

For the binding studies, Ser^{26} depsipeptide *iso*-Aβ (1–42) was used, which was synthesized and purified as described previously[132]. The lyophilized *iso*-Aβ (1–42) was dissolved in MilliQ water in a concentration of 1 mg mL^{-1}, sonicated for 3 minutes and the pH was set to 7.0 to initiate an O to N acyl migration, whereby the native sequence can be readily formed. The sample was incubated at room temperature for 10 minutes. Then the pH was set to 11 and the sample was kept at room temperature for additional 2 hours. After the incubation, the Aβ stock solution was aliquoted and stored at –20 °C until use. To obtain Aβ oligomers, the aliquot of 1 mg mL^{-1} was diluted to a final concentration of 50 μM with 26.67 mM PBS and the pH was set to 7.4 with 1 M HCl. The sample was incubated at 37 °C for 3 hours. To calculate the accurate concentration of the Aβ solution, the peptide content of the lyophilized *iso*-Aβ (1–42) was determined by amino acid analysis, and it varied typically between 70–80%. Exact peptide concentrations of the stock solution were calculated by taking these data in consideration.

3.3. ELISA experiments

PIERCE (Rockford, IL, USA) avidin (125 pmol/well or 60 pmol/well) coated plates were used for the ELISA experiments. The capture molecule was dissolved in phosphate buffer saline (PBS) at a concentration of 10 mg ml^{-1}, and 100 μl capture molecule solution was pipetted in

each well and incubated for 2 hours at room temperature. The plate washed three times with 200 µl TPBS [20 mM PBS containing 1% bovine serum albumin (BSA) and 0.1% TWEEN20] was incubated with 100 µl diluted amyloid solution under shaking (overnight, 4 °C). After washing the plate three times with 200 µl TPBS, the primary antibody (6E10, Covance, Leeds, UK) was diluted with the washing buffer (1:10000 dilution) and 100 µl diluted primary antibody solution was pipetted into each well. The sample was incubated for 1 hour at room temperature. The plate was washed three times with 200 µl TPBS and 100 µl of the secondary antibody Histols-M (Histopathology Ltd., Pécs, Hungary) in 1:250 dilution or anti-mouse IgG HRP (Dako, Glostrup, Denmark, 1:10000 dilution) was pipetted to each well. After 1-hour incubation at room temperature, the plate was washed twice with 200 µl TPBS (in the first washing step the TPBS solution was left in the plate for 30 minutes). Development was carried out with 100 µl 3,3',5,5'-tetramethylbenzidine (TMB) solution pipetted into each well and the absorbance was measured with a plate reader (NOVOstar OPTIMA, BMG Labtech, Offenburg, Germany) in plate mode, for approximately 1.5 hours. For validation, Innotest® β-amyloid (1–42) (Innogenetics, Gent, Belgium) assay was performed according to the manufacturer's instructions.

3.4. ITC experiments

Isothermal calorimetric titrations were performed with a Microcal VP-ITC microcalorimeter in pH 7.4 PBS buffer solution. In individual titrations, 10 µL portions of the solution containing the ligand were repeatedly injected from the computer-controlled 300-µL microsyringe at intervals of 300 s into the Aβ oligomer solution prepared in the same buffer as the ligand. All measurements were carried out at 285 K. The Aβ concentration in the cell was 100 µM and the total ligand concentration was 250 µM in the syringe. The titration was stopped when the precipitation of the Aβ aggregates became excessive.

For ITC analysis of the CaM–foldamer interaction, 20 mM HEPES with 30 mM $CaCl_2$, pH 7.0 was used as a buffer. Peptide solutions were sonicated for 20 minutes before titration to avoid aggregation. The foldamer solution (10 or 15 µl) was injected from the computer-controlled microsyringe into the CaM solution at intervals of 240 s. The CaM concentration in the cell was between 3 and 7 µM, and the concentration of foldamers in the syringe was 85–200 µM. The temperature was adjusted to 298 K. Control experiments were performed by injecting the ligand into a cell containing buffer with no target, and the heats of dilution were subtracted from those measured in the presence of the protein. The experimental data were fitted to the two independent binding site model by using a nonlinear least-squares procedure, with

ΔH_b, $\Delta H_{b'}$, K_d, $K_{d'}$ (dissociation constants), n and n' (number of binding sites for monomer), as adjustable parameters.

3.5. Pulldown assay

Screening of the folded fragment library with CaM was carried out by pulldown assay. 100 µl of 50 w/v% cobalt affinity resin suspension (TALON, Takara Bio USA, Inc., Mountain View, CA) was pipetted into a paper filter spin cup (Thermo Scientific), centrifuged at 1000 RPM for 2 minutes, and washed three times with 300 µl of 20 mM HEPES buffer (pH 7.4), which contained 150 mM NaCl and 1 mM $CaCl_2$. Polyhistidine-tagged CaM was conjugated to the resin at a 2 mg ml^{-1} concentration, and the mixture was shaken at 100 RPM at room temperature for 30 minutes. After the conjugation, the resin was washed three times with the buffer to remove excess protein, and then it was incubated with the foldamer sublibrary, where each library member was in a concentration of 1 or 10 µM in two different experimental setups. The library with the immobilized CaM was also shaken at 100 RPM at room temperature for 30 minutes. The unbound fragments in the supernatant were removed from the resin for further analysis (unbound fraction, UF) and then 200 µl of 200 mM imidazole was added to the sample to elute the polyhistidine-tagged CaM and bound library members from the resin at room temperature for 5 minutes. Then, it was centrifuged as described previously. Negative control experiments were carried out using the same procedure in the absence of polyhistidine-tagged CaM to measure the nonspecific binding between the resin and the foldamer library. Collected samples were measured using HPLC-MS and Thermo Xcalibur 2.2 software was used for peak identification and integration. On the basis of HPLC-MS peak integration, relative fragment content (RFC) in the protein complex was calculated for each library member using the following formula:

$$RFC\ (\%) = \frac{c_{i,complex}}{\sum_{i=1}^{n} c_{i,complex}} \times 100$$

where n is the total number of library members, $c_{i,complex}$ is the concentration of the fragment *i* in complex with the protein. The latter value was calculated for each library member by using the following equation:

$$c_{i,complex} = c_0 \times (1 - unbound\ fraction\ (UF_i)),$$

where c_0 was equal with the initial concentration (1 or 10 µM) of the given fragment *i*. UF_i was calculated from the ratio of *i* in the supernatant and in the control sample:

$$UF_i = \frac{AUC_{i,supernatant}}{AUC_{i,control}}$$

where $AUC_{i,\ supernatant}$: area under the curve of the given fragment (*i*) in the supernatant, $AUC_{i,\ control}$: area under the curve in the control sample.

3.6. Generation of dynamic combinatorial library

DCLs were prepared from Cys-functionalized building blocks each at a concentration of 10 μM in a redox buffer [pH=7.4, 20 mM HEPES, 150 mM NaCl, 1 mM $CaCl_2$, 3 mM NaN_3, 500 μM reduced glutathione (GSH), 125 μM oxidized glutathione (GSSG)]. CaM was used as a template in three different concentrations: 1 μM, 6 μM, 30 μM and a control DCL was started in the absence of template protein in parallel. Library was shaken at 37 °C, 250 RPM for 5 days in Eppendorf LoBind microcentrifuge tubes. At the beginning and every 24 h, 100 μl of reaction mixtures were taken for analysis and quenched with an equivalent volume of 10% TFA in water. All quenched reaction mixtures were analyzed using HPLC-MS, and library members were identified according to their mass and hydrophobic characteristics. Amplification factors (AFs) were determined as the component concentration ratio relative to the control experiment: $AF_i = AUC_{i,\ CaM} / AUC_{i,\ control}$, where $AUC_{i,\ CaM}$: AUC of compound *i* in the presence of CaM, $AUC_{i,\ control}$: AUC of compound *i* in the control sample (without CaM).

3.7. LC-MS methods and peak detection parameters

HPLC/ESI-MS analysis was used to characterize the samples from the pulldown assay and the composition of DCLs. LC-MS analysis was performed with a Thermo Scientific Dionex UltiMate 3000 HPLC system interfaced to an LTQ ion trap mass spectrometer (Thermo Electron Corp., San Jose, CA, USA). Samples were injected onto a Phenomenex Aeris Widepore XB-C18 (250 × 4.6 mm, particle size: 3.6 μm, pore size: 200 Å) analytical HPLC column using gradient elution 5–80% solution B during 25 minutes with a flow rate of 0.7 mL min^{-1}. For pulldown samples, eluent compositions were 0.1% acetic acid in distilled water (solution A) and 0.1% acetic acid in acetonitrile (solution B). DCL samples were measured at 50 °C column temperature with 0.1% formic acid in distilled water used for solution A and 0.1% formic acid in acetonitrile for solution B. Mass spectra were acquired in full scan mode in the 200 to 2000 m/z range. For overlapping peaks, selective reaction monitoring (SRM) was used.

Thermo Xcalibur 2.2 software package was used for peak identification and integration. 83% of the foldameric fragments could be resolved separately *via* HPLC-MS/MS measurements

based on molecular weight, MS fragmentation pattern, and retention time considering the relative hydrophobicity of the side chains. Most of the unresolved peaks were foldamers that contained β^3hIle or β^3hLeu in position 5. These were integrated and averaged. Using ICIS peak detection algorithm[133], the general detection and integration criteria were the following: smoothing points 5, baseline window 80, area noise factor 5, peak noise factor 10. Using these processing setups, all raw data files were reprocessed together and analyzed. Errors in peak identification during the automatic processing were corrected manually.

3.8. NMR experiments

Structural analysis of the foldamers. Peptides were dissolved in 20 mM pH 7.0 d_{18}-HEPES (90% H_2O, 10% D_2O) containing 0.02% NaN_3 and 30 mM $CaCl_2$ at concentrations of 90–500 μM, depending on the solubility of the compound. NMR experiments were performed at 298 K. 2D TOCSY measurements were carried out with homonuclear Hartman–Hahn transfer with a mixing time of 80 ms (DIPSI2 sequence). 2D ROESY spectra were recorded with a mixing time of 400 ms. The number of scans varied between 8 and 64, depending on the concentration of the sample. In order to assess the bound conformation of the ligands, 0.02 equivalent CaM was added to the samples and 2D NOESY spectra were recorded with a mixing time of 150 ms. Control NOESY spectra were recorded in the absence of the protein.

^{15}N HSQC titration experiments. Titration experiments were carried out on a Bruker Avance III 600 MHz spectrometer equipped with a 5 mm CP-TCI triple-resonance cryoprobe. $^{15}N/^{13}C$ CaM (Creative Biolabs, Shirley, NY, USA) was dissolved in 20 mM pH 7.0 d_{18}-HEPES buffer (90% H_2O, 10% D_2O) containing 30 mM $CaCl_2$ and 0.02% NaN_3. Reference 2D heteronuclear ^{15}N-HSQC spectrum was acquired for the ligand-free CaM at a concentration of 45 μM at 30 °C with 256 increments and 16 scans. Foldamers were added to the $^{15}N/^{13}C$ CaM sample in solid form (aliquoted and lyophilized from solutions) and ^{15}N-HSQC spectra were measured again in the presence of the foldamers, resulting in a series of CaM spectra with 0.5, 1.0, 1.5, 2.0, 3.0 and 4.0 equivalent peptides. Chemical shift assignment was based upon literature data and verified by standard triple-resonance NMR experiments. Processing was carried out by using Topspin 3.5 (Bruker) and processed data were analyzed with Sparky 3.114 (T. D. Goddard and D. G. Kneller, SPARKY 3, University of California, San Francisco). The chemical shift perturbation (CSP) values were calculated by using the formula $[(\Delta\delta(^1H))^2 + 0.14*(\Delta\delta(^{15}N))^2]^{1/2}$.

4. Results and Discussion

4.1. Recognition of β-amyloid oligomers with multivalent foldameric conjugate

From the aspect of molecular recognition, two major strategies can be followed to discriminate soluble aggregated Aβ from monomers in a sandwich-based biochemical test: i) application of a conformation-specific antibody as a capture antibody, ii) using the same sequence specific antibodies as the capture and the detection antibody at the same time. In the latter case, the concept is that two antibodies are only able to bind to the same antigen if there are multiple epitopes displayed. For Aβ, this is possible through aggregation. The antibody-based Aβ capture schemes may cause false positives, because of the cross-reactivity of the capture molecules[134]; therefore, alternatives are sought to replace them. Taking advantages of fragment-based approach and surface mimetic properties of small ordered foldameric fragments, multivalent ligand was designed against Aβ42 oligomers[98]. Solvent exposed $K^{16}LVFFAE^{22}$ sequence of the amyloid was the starting point for bottom-up design of the recognition unit. We hypothesized that a basically hydrophobic molecule, which can form salt-bridges with the complemetary part of the amyloid sequence, may selectively recognize the growing end of the oligomer. Testing a small set of pure β- and α/β- peptides, a hexameric 14-helix proved to be the best for amyloid recognition containing β^3hArg and β^3hAsp at position 2 and 5 of a scaffold based on (1*S*,2*S*)-2-aminocyclohexanecarboxylic acid (ACHC) (Figure 5, **H1**). The 14-helix is frequently applied template for proteinogenic side chain presentation, because three faces can be separated on its surface. In the case of **H1**, one face is for epitope presentation and two faces to form hydrophobic shield to protect ion-pairing interactions from water. Binding affinity of **H1** towards Aβ was tested with different biochemical assays and it was successfully enhanced by coupling multiple copies of foldamers to a tetravalent zero generation poly(amidoamine) (G0-PAMAM).

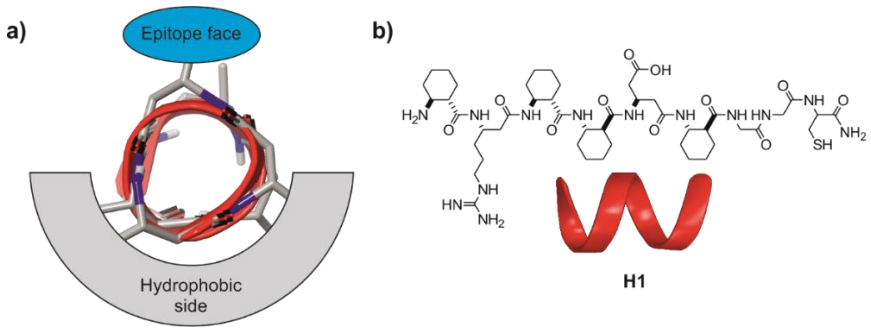

Figure 5. Structure of the foldameric recognition element: **a)** faces of the 14-helix projecting the proteinogenic side chains towards a surface, **b)** schematic representation and structural formula of **H1**.

4.1.1. Design of the affinity assay for Aβ detection

The multivalent foldameric conjugate mentioned above displayed low nanomolar binding affinity toward Aβ oligomer, which is comparable to the antibody–antigen interactions. In order to take advantage of this artificial antibody mimetic, our goal was to develop an easy-to-perform sandwich assay for selective detection of soluble Aβ oligomers. The general experimental setup of a sandwich ELISA assay (Figure 6) consists of a highly specific capture element, an antigen, a detection antibody for the recognition of antigen. and a secondary antibody suitable for colorimetric detection.

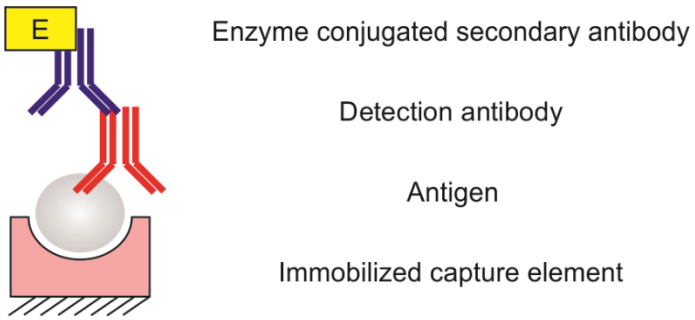

Figure 6. Schematic representation of the sandwich ELISA setup.

Our work focused on the optimization of the capture molecule and the immobilization strategy, which is based on the multivalent foldamer conjugate recognition element. For detection antibody, we utilized the anti-Aβ monoclonal mouse antibody 6E10, a commonly applied tool in Western blot techniques, immunhistochemistry, and ELISA. It recognizes the N-terminal end (residues 1–16) of Aβ, which segment is disordered and accessable even in the aggregated form. Accordingly, the secondary antibody was a horseradish peroxidase (HRP)-conjugated anti-mouse antibody, where HRP was responsible for colorimetric detection. As a substrate of the enzyme, 3,3',5,5'-tetramethylbenzidine (TMB) solution was choosen, that undergoes oxidation by HRP enzyme yielding 3,3',5,5'-tetramethylbenzidine diimine with color change from yellow to blue.

4.1.2. Structural optimization of the capture element

As a first step of the optimization, the fine-tuning of the structure of the foldameric conjugate was carried out in two aspects. We investigated i) the effects of multivalency and geometry of the template and ii) the effects of the amino acid replacements in the sequence of the foldameric recognition fragment on Aβ binding.

4.1.2.1. Effects of multivalency and the geometry of the template

Sensitivity is a crucial parameter in the detection of Aβ aggregates. Because their concentration in body fluids is in the picomolar range in the early stage of AD[135], high-affinity

interaction is required for amyloid recognition. To further increase the amyloid binding efficiency and examine the effects of multivalency on Aβ binding, multiple **H1** foldamers were coupled to different scaffolds. In this work, the identifiers of the compounds consist of four digits: 1. symmetry (**C**: central, **F**: focal) – 2. valency of the conjugate (2–8) –3. and 4 – **H** and the number of the recognition unit (**1**–**9**). Any kind of tags directly attached to the scaffolds are indicated at the beginning of the compound names, and tags at the N-terminal of the foldamer are indicated at the end of the identifier. Besides the di- and tetravalent-conjugates studied previously (Table 2, **C2-H1** and **C4-H1**), tri- and octavalent conjugates were designed having central symmetry (**C3-H1** and **C8-H1**). It was reported earlier that a foldameric fragment alone (**H1**) and a divalent ligand (**C2-H1**) can show low micromolar and submicromolar (high nanomolar) interaction with Aβ sample, respectively. For trivalent compound **C3-H1**, low nanomolar K_D was obtained close to the dissocation constant of the tetravalent conjugate **C4-H1**. In addititon, it showed two-stage interaction with Aβ oligomers in isotermal titration calorimetric (ITC) measurements. Good correlation was found between the binding affinities and the valencies of the conjugates. Interestingly, however, the increase of the number of arms from four to eight did not improve the affinity further (Table 2). From the stoichiometry data, it was transparent that **C4-H1** makes a 1:4 high-affinity complex with Aβ (referenced to the concentration of the monomers) at the first binding stage, and the high-affinity interaction does not require more than four foldameric capture segments.

Table 2. Effects of multivalency on Aβ binding.

Conjugate	**Scaffold**	**Valence**	**K_D (nM^{-1})***
H1	-	1	2376.1 ± 214.4
C2-H1	1,4- di(maleimido)butane	2	721.4 ± 120.1
C3-H1	tris(2-(5-aminopentanamido) ethyl)amine	3	18.5 ± 13.9[1] 155.0 ± 130.9[2]
C4-H1	generation zero poly(amidoamine) dendrimer	4	6.9 ± 1.4[1] 281.1 ± 38.7[2]
C8-H1	generation one poly(amidoamine) dendrimer	8	69.0 ± 12.0[1] 193.4 ± 30.5[2]

*based on ITC experiments
[1] and [2] belong to the first and the second binding stages
„**C**" in the name of the compound refers to the central symmetry and the number indicates the valency

In sandwich ELISA experiment, the antibody is usually immobilized on the surface of a 96- or 384-well plate by passive adsorption. The Fc region of the protein is generally more hydrophobic and, therefore, more likely to be absorbed, than the Fab region, which remains

mostly accessable to the antigen. In the case of a synthetic molecule, oriented immobilization is particularly essential to ensure effective analyte binding. Avidin–biotin is known as one of the strongest and most specific non-covalent interaction in nature, with dissociation constant in the femtomolar range (K_D= 1.3 x10^{-15} M at pH 5.0)[136]. It has been exploited in the detection of many biomolecules, purification techniques, and labelling strategies. Using this interaction in the immobilization is especially preferred in our case due to the small size of biotin, which can be easily coupled to the peptide even by solid-phase peptide synthesis. During optimization, two biotinylation strategies were followed. First, biotin-tag was directly coupled to the N-terminus of the foldamer sequence, which gave **H1-B,** and then it was conjugated to G0-PAMAM dendrimer having central symmetry (Figure 7, **C4-H1-B**). Second, biotin-tag was placed in the focal point of an oligo-L-lysine dendron by coupling N-ε-biotinyl-L-lysine (**B-F4-H1**). Figure 7 represents the major structural differences between these two scaffolds.

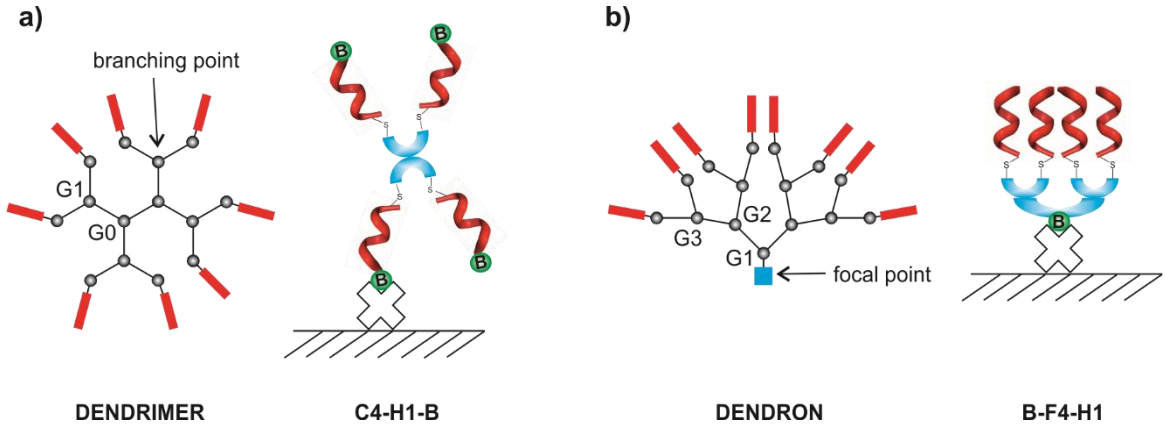

Figure 7. Schematic representation of the branched templates: **a)** centrally symmetric dendrimer and **C4-H1-B** conjugate immobilized on a surface, **b)** dendron having a focal symmetry and arrangement of the foldamer helices in immobilized **B-F4-H1**, where **F** refers to focal symmetry.

Binding efficiencies of the capture elements were quantified in ELISA experiments and significant differences were found. EC_{50} value for **C4-H1-B** was 648.5 ± 11.2 nM and for **B-F4-H1** the EC_{50} was three orders of magnitude lower (0.97 ± 0.04 nM) indicating higher affinity towards Aβ sample (Figure 8). Both dendrimers and dendrones are fully branched in the solution phase. However, it is likely that biotinylation at the root of a lysine-dendron yields an immobilized conjugate, in which the helical units may freely point away from the surface. In contrast, **C4-H1-B** uses one of its foldamer fragments to anchor the conjugate to the surface, which prevents presenting all foldamer helices toward the solution phase necessary for high-affinity binding. Another possible reason for the decrease in efficiency can be that biotinylation capped the free N-terminal amino group of the foldamer, which may have critical role in recognition. In order to confim this hypothesis, an N-terminal acetylated form of the recognition

fragment (Figure 9, **H1-Ac**) was synthesized and linked to tetravalent lysine dendron (**B-F4-H1-Ac**). In ELISA experiment, we measured increased EC_{50} value (30.16±2.27 nM) for the acetylated conjugate compared with the non-acetylated one, which highlighted the importance of the free N-terminals in high-affinity binding. Since it was still better than **C4-H1-B** we could conclude that the accessibility of all four foldamer arms is also an essential requirement.

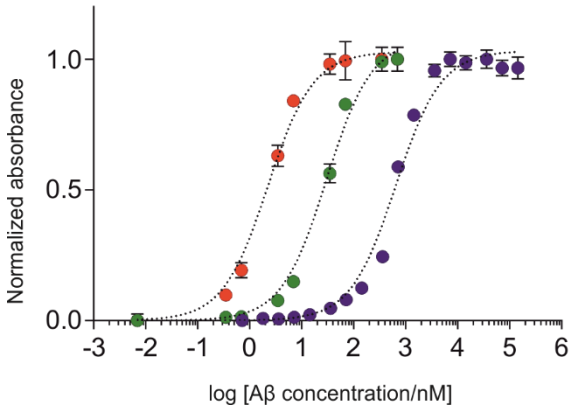

Figure 8. Results of the ELISA experiments. Comparison of the affinities of the immunoassay for **C4-H1-B** (red), **B-F4-H1-Ac** (green), and **B-F4-H1** (blue) as capture elements. Absorbances were normalized to the maximum value in each experiment.

4.1.2.2. Effects of side shain alterations in the foldamer segment on Aβ binding

Although the number of arms of the multivalent conjugate and the topology of the scaffold is crucial for high-affinity binding, only the foldameric fragments are responsible for selective recognition of the Aβ oligomers. To study the role of certain structural elements of the foldamer in the binding, a set of new foldamer sequences was designed and attached directly to a biotinyl-tetravalent oligo-L-lysine dendron (**B-F4**) to make them applicable in ELISA as capture molecules.

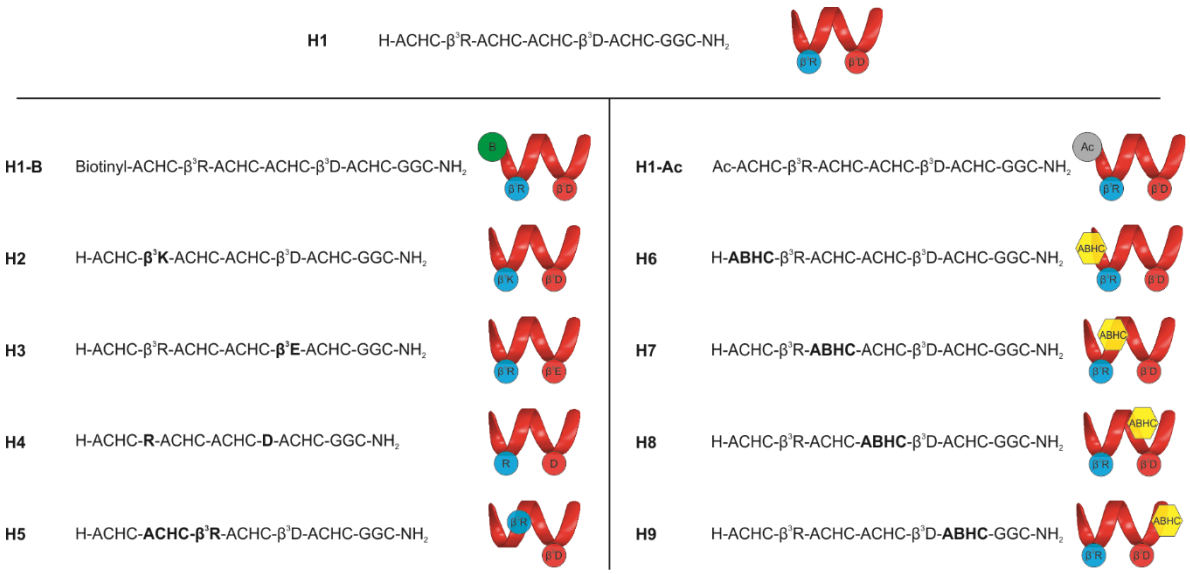

Figure 9. Compounds designed for Aβ recognition. Identifier, sequence, and schematic representation of the recognition units.

Structural changes included fine-tuning the properties of the proteinogenic side chains (**H2/3/4**), changing the relative position of ionic residues (**H5)**, and introducing bulky bicyclic side chains in different positions (**H6/7/8/9**). Binding affinites of biotinyl–tetravalent conjugates (**B-F4-H1/2/3/4/5/6/7/8/9**) were tested in ITC and ELISA experiments. In the cases where the ITC curve fitting failed due to low heat response or poor solubility, only the ELISA results provided information about the binding. As **B-F4-H1** contains the initial binding sequence, the effectivities of the further conjugates were compared to it. All evaluated ITC results showed two-stage binding behavior as in the case of **F4-H1**. In comparison with the biotinylated version, the binding affinites are similar low nanomolar in ITC, which supports that biotin has a negligible effect in the solution-phase binding assay.

Table 3. Thermodynamic parameters resulting from ITC analysis for conjugates and estimated EC_{50} values from quantitative evaluation of ELISA experiments.

Compound	K_D (nM^{-1})	ΔG (kcal M^{-1})	ΔH (kcal M^{-1})	-TΔS (kcal M^{-1})	EC_{50} (nM)
B-F4-H1	27.63 ± 7.74[1]	- 9.97	51.33	61.30	0.95 ± 0.06
	239.62 ± 68.67[2]	- 8.73	0.31	9.04	
B-F4-H2	53.20 ± 38.70[1]	- 9.59	6.57	16.16	5.36 ± 1.42
	373.40 ± 104.33[2]	- 8.78	0.64	9.42	
B-F4-H3	2.53 ± 1.81[1]	-11.34	1.96	13.30	1.92 ± 0.21
	175.20 ± 46.41[2]	- 8.91	0.76	9.67	
B-F4-H4	nd	nd	nd	nd	7.70 ± 3.06
B-F4-H5	nd	nd	nd	nd	2.71 ± 0.21
B-F4-H6	19.30 ± 9.40[1]	- 10.17	2.48	12.66	1.79 ± 0.09
	816.40 ± 466.90[2]	-8.03	0.27	8.30	

B-F4-H7	34.10 ± 10.00[1]	- 9.85	4.88	14.73	1.34 ± 0 04
	652.30 ± 158.50[2]	- 8.16	0.37	8.53	
B-F4-H8	8.61 ± 5.64[1]	-10.64	7.39	18.02	1.35 ± 0.08
	78.99 ± 45.92[2]	-9.37	0.35	9.72	
B-F4-H9	nd	nd	nd	nd	1.59 ± 0 08

nd= not determined. [1]K_D belongs to the first binfing stage. [2]K_D belongs to the second binding stage.

It has been shown previously, that removal of the ionic residues of the foldamer fragment (replacement of both β^3hArg and β^3hAsp to β^3hSer) resulted in a K_D value with one order of magnitude higher[98]. Homologous replacements of the charged side chains modulated the affinity, but they could be basically tolerated. The β^3hArg to β^3hLys exchange (**B-F4-H2**) caused a decreased affinity at the first binding stage, whereas the change of β^3hAsp to β^3hGlu (**B-F4-H3**) led to somewhat improved properties in ITC. The effects of the β^3hArg to β^3hLys replacement can be explained by the structural differences between the charged side chains. In contrast to Lys, where the charge is localized on the terminal aliphatic amino group, the positive charge of Arg is delocalized within the π-bonded system of the guanidinium ion, resulting in a considerably different charge distribution and geometry. This makes arginine capable of multiple types of favorable interactions; thus, Arg is preferred as hot-spot residue compared to Lys[137]. For **B-F4-H3**, the results suggested that the presence of the negatively charged residue in position 5 is essential for the binding[98], but the length of the side chain did not have an important role. In the ITC experiment of **B-F4-H4**, in which we changed β^3hAsp to Asp, and β^3hArg to Arg, the observed low ΔH made the analysis difficult. A similar low-heat response was found for **B-F4-H5**, where we changed the position of the positively charged residue (β^3hArg) in the helix, resulting in failed fitting. A systematic ACHC to (1*S*,2*S*,3*S*,5*R*)-3-amino-6,6-dimethylbicyclo[3.1.1]heptane-2-carboxylic acid (ABHC) replacement was also carried out along the chain (**B-F4-H6/7/8/9**), and we found that this approach did not lead to a significant increase in the affinity in the first binding stage (Table 3). C-terminal ACHC to ABHC replacement in the helix (**B-F4-H9**) considerably decreased the solubility of the conjugate, which made the dissolution difficult and, therefore, K_D could not be determined under these conditions.

The EC_{50} values for the complete set of new conjugates were calculated individually from the data of the ELISA experiments as well. Comparing the EC_{50} values of **B-F4-H6/7/8/9**, the replacement of ACHC to ABHC had only a minor effect on the Aβ binding. The cyclic β-amino acid ACHC not only stabilizes the helical conformation of such a short foldamer, but also shields the electrostatic interactions from the solvent upon binding, due to its bulky nature.

Increasing the bulkiness of the helix by a substitution of ACHC with a bicyclic amino acid in the recognition element resulted in a retained binding affinity to Aβ. On the other hand, changing only one ACHC to ABHC in the foldamer sequence significantly decreased the solubility of the conjugate. In the ELISA experiment, the EC_{50} values for **B-F4-H4** and **B-F4-H5** could be determined observing increased values compared with **B-F4-H1**. For **B-F4-H4**, the results indicated that the simultaneous replacement of β^3hArg and β^3hAsp to the α-analogues could be moderately tolerated. The β^3 to α exchange gave βαββαβ backbone pattern that could alter the folding behaviour of the hexamer[87]. This finding revealed the importance of the conformation of the helical recognition segment. Interestingly, changing the relative position of the charged residues (**B-F4-H5**) within the helix did not influence the binding of the molecule to Aβ considerably. Consequently, some flexibility may be assumed regarding the structure of the foldamer. Since we did not find more effective recognition unit, **B-F4-H1** was used as a capture element for further optimization of the enzyme-linked immunoassay.

4.1.3. Detection of Aβ oligomers in ELISA

Since the concentration of the Aβ oligomers in the early stage of AD is in a low picomolar range, a highly sensitive method was needed for quantitative measurements. The quantification of the foldamer–amyloid complex was achieved by measuring the absorbance of TMB diimine at 370 nm. With a large excess of substrate present, the recorded intensity depended on the concentration of the enzyme, but the ratio of HRP to antibody was constant for a given batch of antibody. Therefore, the amount of the enzymes taking part in the colorimetric reaction could not be further increased by enhancing the concentration of the secondary antibody. An HRP-polymer tagged secondary antibody (Histols-M) increased the sensitivity of the system due to the higher number of HRPs bound to the polymer. As a result, we found intense immunostaining without background (Figure 10a). Another important parameter influencing sensitivity is the steric hindrance between the immobilized capture molecules, which may limit the performance of the detection. The effects of steric crowding were tested by the variation of the surface coverage. Experiments were carried out with plates precoated by streptavidin with surface loads of 60 pmol and 125 pmol per well. Although the EC_{50} value did not change with the surface load, higher intensity was recorded for the 60 pmol plate (Figure 10b) indicating that it is the HRP-polymer tagged secondary antibody, which performs better if steric hindrance is decreased.

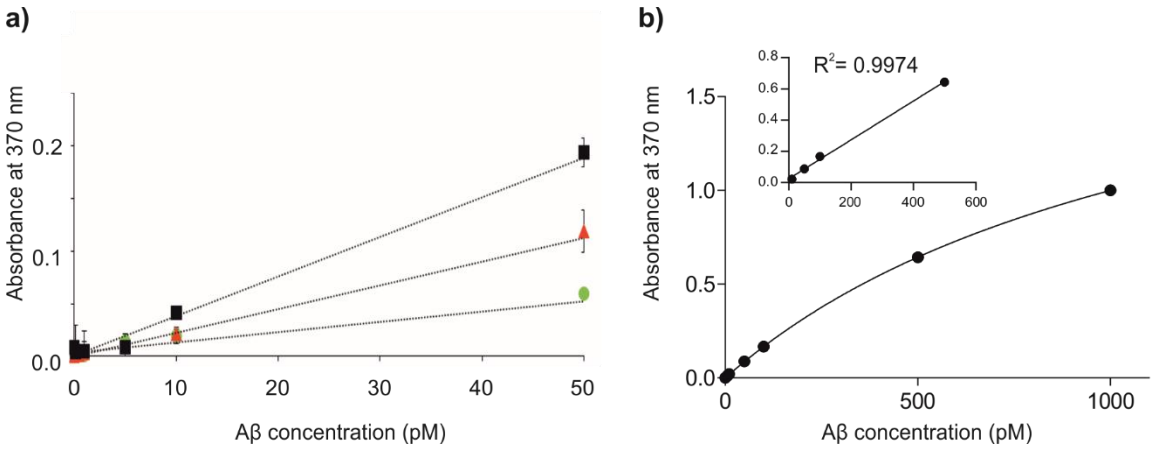

Figure 10. Optimization of the ELISA setup. **a)** recorded absorbance values at 370 nm as a function of Aβ concentration: green circle: initial conditions (surface loading: 125 pmol well^{-1}; HRP-conjugated secondary antibody), red triangle: surface loading: 125 pmol well^{-1}, Histols-M secondary antibody; black square: surface loading: 60 pmol well^{-1} plate, Histols-M secondary antibody. **b)** Result of the ELISA experiment using the optimized conditions; the inset shows the linear dependence of intensity on Aβ concentration between 10–500 pM.

Utilizing the improved capture ligand **B-F4-H1** and the optimized protocol, the limit of detection (LOD, defined as three times the standard deviation of the blank) was estimated to 5 pM (n= 12), and linear dependence of intensity on Aβ concentration was found over the concentration range 10–500 pM (Figure 10b, R^2 = 0.9974).

The selectivity of the assay toward the Aβ oligomers was tested using both predominantly monomeric and oligomeric Aβ samples. The Aβ solutions with different aggregation states were prepared according to literature protocols[98]. The monomeric and oligomeric samples were checked in parallel with a commercially available Aβ monomer-selective ELISA kit (Innotest®) commonly utilized in clinical studies. For ELISA performed with the capture element **B-F4-H1**, concentration-dependent signal was observed for the oligomeric sample in the range 0–200 pM (Figure 11a). The fresh monomeric Aβ did not yield signal in this concentration range (LOD estimated to be 3600 pM). In contrast, the monomer-sensitive commercial sandwich ELISA kit produced concentration-dependent signal for the monomeric Aβ sample (Figure 11b). At the same time, a relatively low-intensity response was detected above 100 pM for the aggregated Aβ sample, which can be attributed to the residual monomeric Aβ content. These results revealed that capture ligand **B-F4-H1** is selective for the Aβ oligomers, and the foldamer-based sandwich ELISA assay gives complementary response to the monomer Aβ selective kit.

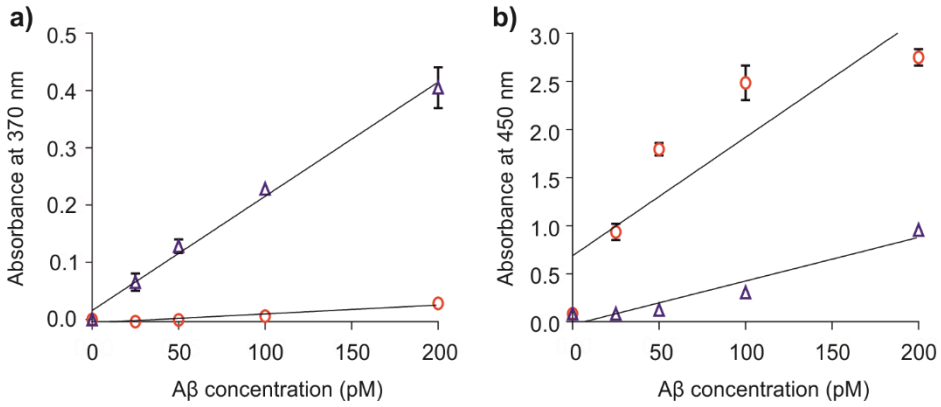

Figure 11. Confirmation of the oligomer selectivity of the assay. Measured signals of the predominantly monomeric samples (red circle) and oligomeric samples (blue triangle) in **a)** the foldamer-based sandwich assay (capture molecule: **B-F4-H1**, detection antibody: 6E10, secondary antibody: Histols-M, recorded signal: absorbance of TMB diimine at 370 nm), **b)** the commercially avaliable ELISA test (Innotest®) designed for the quantitative determination of Aβ42 in human CSF (capture antibody: 21F12 monoclonal antibody, detection antibody: biotinylated 3D6 antibody and HRP-labeled streptavidin, recorded signal: absorbance of TMB diimine stabilized with 0.45 M H_2SO_4 at 450 nm).

It was also reported earlier that foldamer conjugate **C4-H1** cannot bind fibrillar Aβ with high affinity in the solution phase, suggesting that our ELISA method is capable of monitoring the aggregation state of an Aβ solution by detecting solely the oligomer content. A standard Aβ aggregation procedure (incubation of a freshly disaggregated Aβ monomer sample at the concentration of 50 μM, 37 °C for 24 hours) was carried out and samples were taken at regular intervals. Samples were diluted to a total Aβ concentration of 500 pM, then applied onto the ELISA plate. The recorded absorbances increased with time, then the intensity reached a plateau after 3 hours (Figure 12), which remained constant until 18 hours, when the absorbance started to decline.

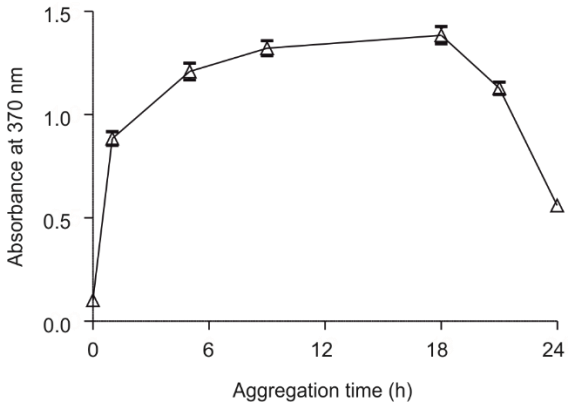

Figure 12. Monitoring time-dependent aggregation of Aβ. Absorbane values were recorded for 500-pM samples diluted *in situ* at each time point.

Towards the end of the experimental run (18 h), aggregation transformed the oligomers and residual monomers to fibrils, which did not show affinity to **B-F4-H1**. These results strongly suggested that this system is able to indicate the state of an ongoing aggregation in a pM sample. This finding, together with the observation that the binding affinity of the tetravalent ligand cannot be improved further by increasing the valence, we could speculate that foldameric conjugate recognizes transient Aβ surface features of oligomers rather than general repeating features of the cross-β-sheet surface of the aggregates. We note that the quantification of fibrillar Aβ is not possible, because of the disaggregation of the pure fibrillar form into oligomeric and monomeric forms[138] at low picomolar concentration. Therefore, selectivity of our foldamer-ELISA assay against the fibrillar form cannot be clearly concluded from these data.

4.2. Bottom-up design approach for recognition of separate hot spots

Calmodulin (CaM) is a commonly used model for protein recognition and inhibition studies[26, 139]. It was selected as a model protein, which has two separate hot spots formed by the symmetrical globular domains, due to its flexibility and structural diversity of its binding partners. Our hypothesis was that the target hot-spot pockets could be mapped using short foldameric segments mimicking the local environment of hot-spot residues in terms of side-chain presentation and solvent shielding (Figure 13a). In order to address the problem of simultaneous optimization of both the recognition segments and the linkage, a dynamic covalent library (DCL) method was developed (Figure 13b).

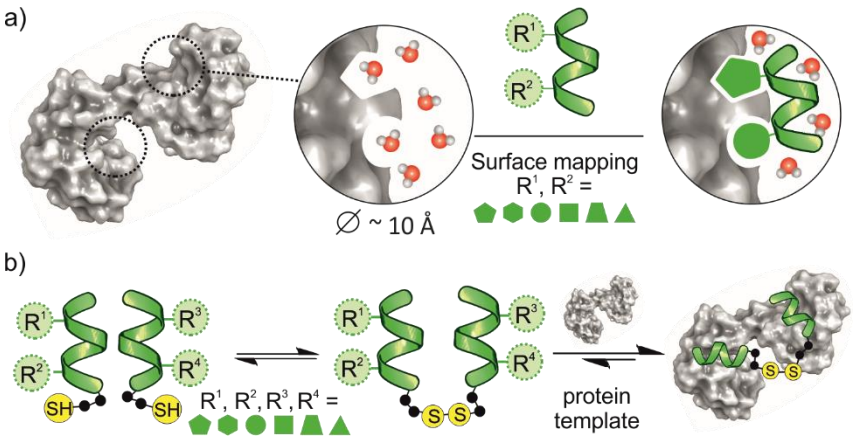

Figure 13. The concept of the foldameric ligand design strategy: **a)** mapping the hot spot pockets of the protein with the helical foldamer library and **b)** optimization of the foldameric ligand using dynamic combinatorial chemistry.

4.2.1. Design of the foldamer library

A 14-helix was used as a template for the presentation of proteinogenic side chains due to its favorable properties mentioned above. The structure of the helix was stabilized by (1*S*,2*S*)-2-aminocyclohexanecarboxylic acid (ACHC) and β^3-homologs of 16 different α-amino acids were placed both to positions 2 and 5 of the hexamer. The variable open-chain residues in juxtaposition pointed into the same direction presenting side chains for molecular recognition. The highly hydrophobic cyclohexane side chains ensure the exclusion of solvent from the shallow binding cleft.

To simplify the production and the HPLC-MS analysis of the 256-membered library, it was divided into four sublibraries each containing 64 members (Figure 14). On the basis of the characteristics of β^3-amino acid at the 2nd position, the sublibraries have aromatic (L1), charged (L2), aliphatic (L3), and polar (L4) side chains.

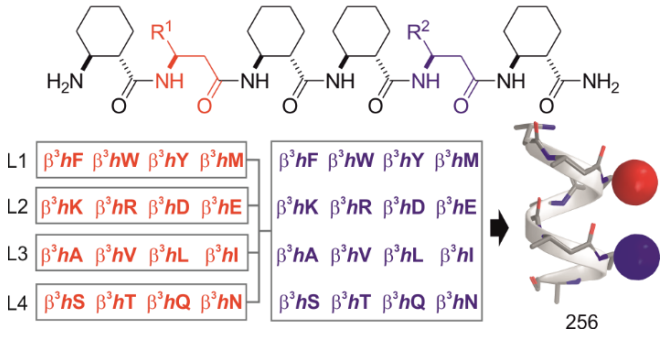

Figure 14. Structural formula and schematic representation of folded segments and the composition of the sublibraries.

The synthesis of the sublibraries was carried out by microwave assisted solid-phase peptide synthesis. To ensure complete representation of each foldamer fragment, double coupling of sub-stoichiometric amount of Fmoc-protected β^3-amino acid mixtures was applied. After purification, each foldameric fragment was identified via HPLC-ESI-MS/MS methods. Taking into account multiple charge states for every single peptide, the purities of the libraries were found between 69–84% (Figure 15) with acceptable equimolarity[140, 141].

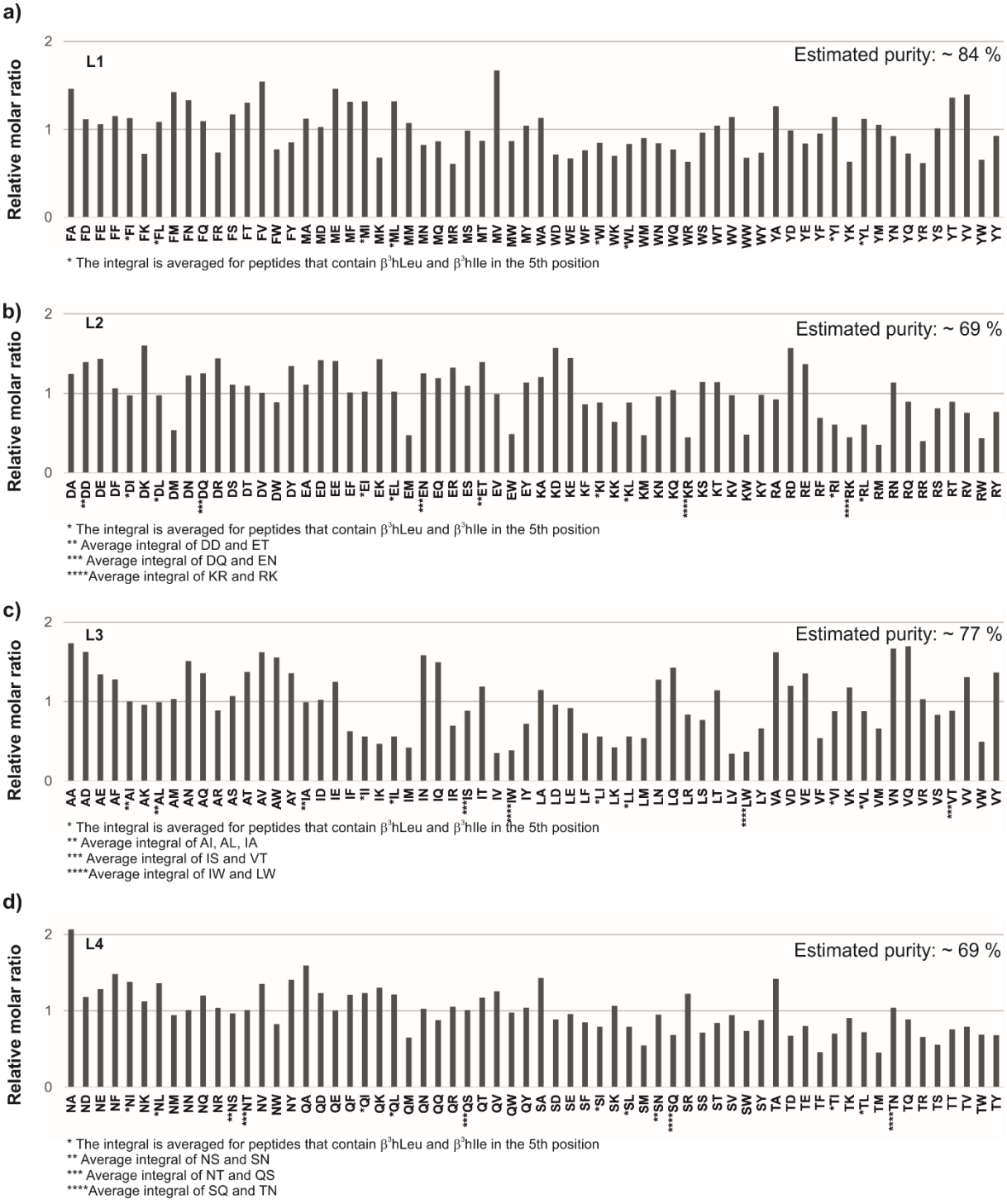

Figure 15. Estimated equimolarity and purity of the 64-membered sub-libraries: **a)** L1, **b)** L2, **c)** L3, **d)** L4. Names of the compounds are generated from the single-letter amino acid codes of the β^3-amino acid used in the position 2 and 5 of the sequence. Equimolarity was calculated using the following formula: $AUC_{compound}/(AUC_{total}/\text{number of library members})$; thus, relative value of 1 indicates equimolar concentration. Purity was estimated using the following formula: $AUC_{compound}/AUC_{total} \times 100$.

4.2.2. Screening of the library members

Generation of a ditopic DCL from 256 peptidic compounds would result in a very complex mixture (theoretically 33280 different compounds). Keeping the concentration of the

fundamentally hydrophobic dimers above the detection limit and their quantification are not possible; thus, careful selection of the members of the DCL is necessary. Therefore, we first ranked the fragments based on their affinity towards CaM in a pulldown assay. Foldamer sublibraries were incubated with the immobilized protein and all unbound fragments were quantified in the supernatant. After the elution of the protein–foldamer complexes, the bound components were analyzed in the eluted fraction as well. In two separate measurements, fragments were applied in two different concentrations. First, the whole library was quasi-equimolar with the protein (library:protein = 1:1), i.e., all fragments have the opportunity to bind to the template without competition. Second, the library was applied in a ten-fold molar access to the protein (library:protein = 10:1) eliciting significant competition between the library members. Foldamers indicated in blue displayed very low tendency to form complexes with CaM (Figure 16). Concerning the acidic characteristic of the protein (pI 4.09), it is not surprising that Glu and Asp side chains are not preferred as hot-spot residues. However, almost all other fragments containing at least one aromatic or aliphatic side chain made complexes with CaM (Figure 16a). Due to the competition between the library members in the 10:1 composition, the enrichment of some fragments increased at the expense of those with lower affinity (Figure 16b). Aromatic side chains are still preferred by the protein especially tryptophan and basic residues containing β^3Arg or β^3Lys in position 2 made stable complexes with CaM. Our results were in line with the known binding partners of CaM[139], as they generally contain Trp residues that fit the Met-rich hot spots of CaM. The enrichment pattern of the fragments depended on the specific composition of the sublibrary. On the basis of results of the pulldown experiments, promising hits were identified to create a focused library for the DCL experiments.

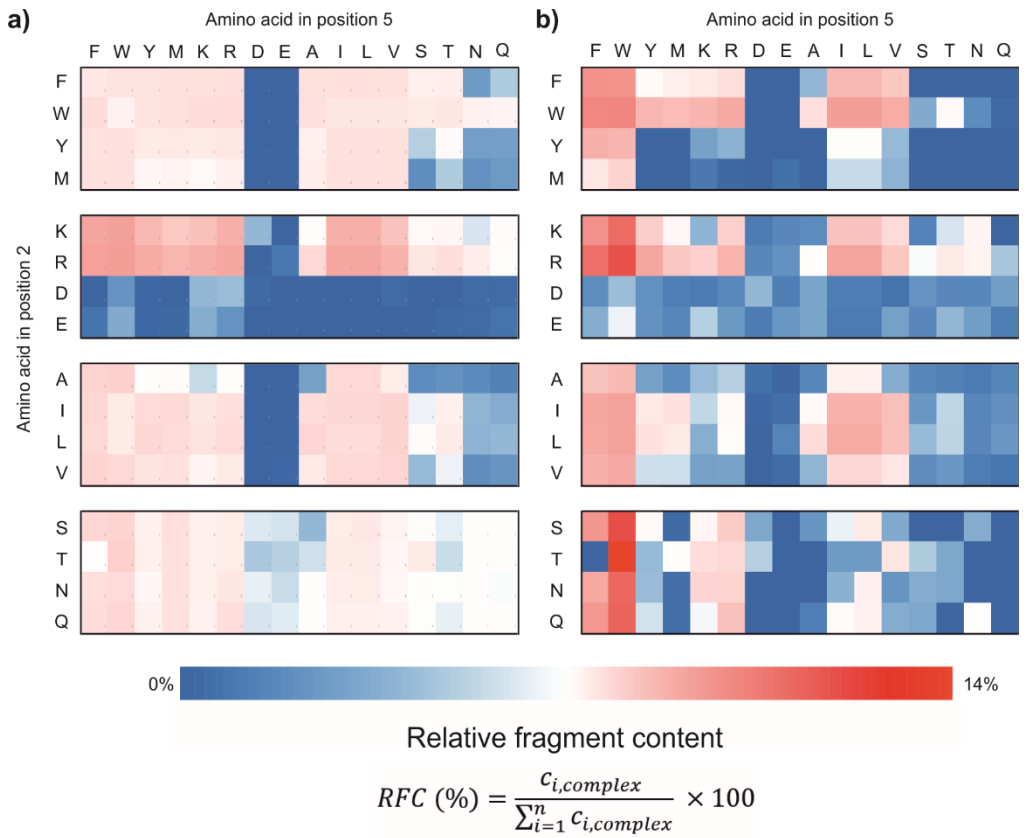

Figure 16. Results of the pulldown assays. Enrichments of the fragments in the protein complexes in two different experimental setups: library-to-protein compositions in **a)** 1:1 and **b)** 10:1. The relative fragment content was calculated for each library member using the indicated formula as described in the experimental section.

4.2.3. Characterization of protein binding with selected foldameric fragments

On the basis of the results of the pulldown assays, the best candidate from each sublibrary was selected to validate and quantitatively characterize the interactions with CaM. The selected foldamers (**WF, RW, LW, TW)** were re-synthesized individually and the nomenclature is according to the standard one-letter codes of the proteinogenic side chains presented by the β^3-residues in positions 2 and 5. In order to investigate the importance of the bulky, ordered secondary structure, a non-helical derivative of **WF** was synthesized (**rrWF**), where the replacement of the 1*S*,2*S*-ACHC in position 4 to its enantiomer pair (1*R*,2*R*-ACHC) prevented helix formation according to the stereochemical patterning approach[17]. ITC experiments were performed to identify the thermodynamic parameters of the binding. Low micromolar-submicromolar K_D values were found (Table 4). The titration curves were fitted against the two independent binding sites model and indicated that CaM binds uniformly two foldamer segments at the same time (Table 4, Figure 17). The non-helical **rrWF** did not show any interaction with the target protein, which highlights the importance of the folding on binding.

The negative ΔH values are accompanied by negative entropy changes for most fragments (Table 4) suggesting multiple favorable noncovalent interactions between the foldameric fragments and the protein. For **LW**, a large negative entropy gain was found accompanied by a positive enthalpy change, suggesting that the interaction is mostly driven by solvophobic effects. The large negative ΔH for **WF** showed that the interaction is enthalpy driven and indicated that the binding is not dominated by the hydrophobic effects, which is an advantageous characteristic for drug design[142].

Table 4. Thermodynamic parameters of fragments binding to CaM.

Compound	$K_{D\ ITC}$ (μM)	n	ΔH	-TΔS	$K_{D\ Trp}$ (μM)*
WF	0.076 ± 0.004	2.11 ± 0.01	-6.79 ± 0.04	-2.41± 0.05	0.065
RW	0.706 ± 0.007	1.97 ± 0.02	-2.72 ± 0.00	-5.40 ± 0.01	1.780
LW	0.139 ± 0.014	1.98 ± 0.03	0.78 ± 0.02	-9.83 ± 0.04	0.514
TW	17.107 ± 1.102	1.82 ± 0.09	-4.3 ± 0.10	-2.0 ± 0.10	n.d.
rrWF	n.d.	n.d.	n.d.	n.d.	n.d.

*estimated K_D from Trp titration experiments

Excitation of Trp-containing peptides results in fluorescence emission in the range 300–400 nm depending on the local enviroment of the indol ring. Upon transfer from solvent-exposed polar enviroment to a hydophobic binding pocket, the emission maximum shifts from 350 nm to 330 nm[143, 144]. Since all selected foldamers contained Trp side chain, we could measure the blueshift of their side chain fluorescence emission to study Ca^{2+} dependency of the interaction and to obtain independent estimation of the K_D of the binding. By titrating the solution of a given fragment with CaM, blueshift was observed for **WF, RW, LW**, and **TW** but not for **rrWF** (Figure 17). The phenomenon was not detected in the absence of Ca^{2+}, which confirmed that the Ca^{2+}-bound active conformation of CaM is essential for the recognition. The estimated K_D values were determined for **WF**, **RW**, and **LW** (Table 4), which showed the same trend as those observed by ITC.

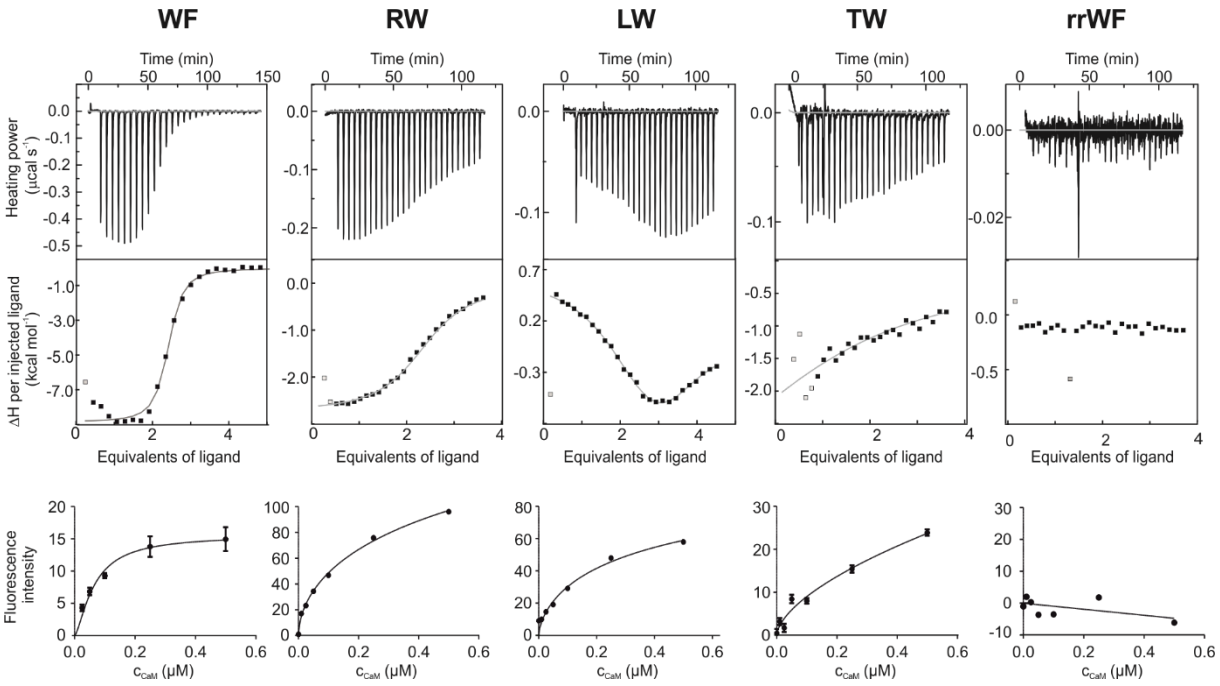

Figure 17. ITC and Trp fluorescence titration data for the selected fragments. ITC titrations showing raw data (upper) and integrated enthalpograms with fitted curves. Bottom line: fitted titration curves for the Trp fluorescence titrations.

The propensity to fold into H14-helix in aqueous buffer was confirmed by ROESY experiments on **WF**, **RW**, **LW**, and **TW** (Figure 18), and long-range i–i+3 inter-residue interactions were detected. Sequence **rrWF** did not show any sign of binding and exhibited disorder in water thus supporting the necessity of the compact and bulky structure for CaM binding.

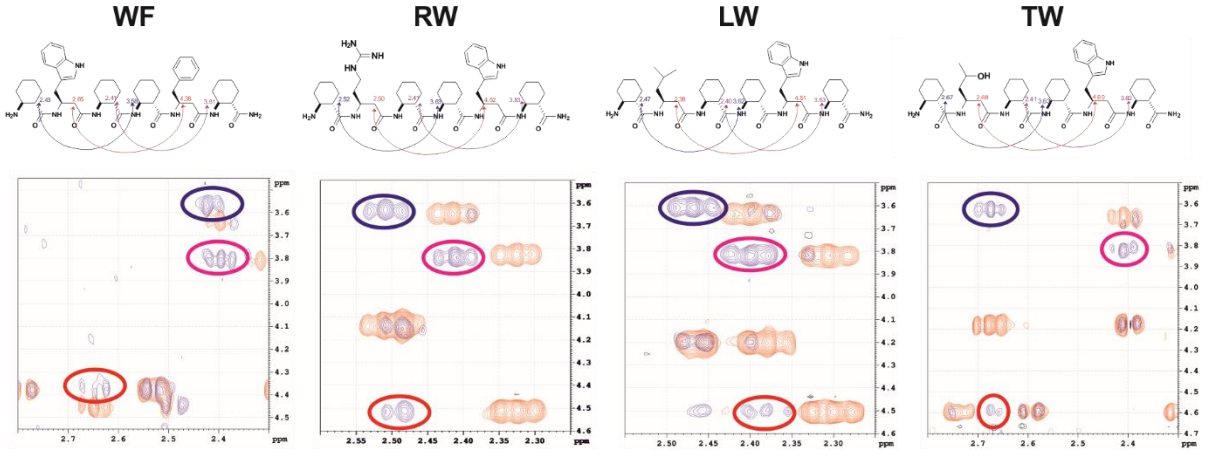

Figure 18. ROESY spectra for foldameric fragments. NOE interactions showing the helicity of compounds. Overlaid TOCSY (red) and ROESY (blue) spectra for compounds in the absence of the protein. Color-coded chemical shift assignment and detected i–i+3 type long-range interactions characteristic for the 14-helix, are indicated on the structures.

RW and **TW**, having micromolar affinities with their fast exchange afforded transferred NOESY (tr-NOESY) measurements, which confirmed the 14-helical conformations in the

bound state as well (Figure 19a, b). In order to locate the binding site of the foldamers, their interactions with CaM were tested with ^{15}N-HSQC NMR spectroscopic titrations, which were conclusive for **RW** and **LW** due to sufficient affinity and signal-to-noise ratio (limited line broadening). Significant chemical shift perturbation (CSP) and/or resonance broadening were observed for target residues L39, M36, M71, M72, M109, M144, and M145 (Figure 19c, e), which are key residues in the CaM–protein contacts and creating the hot spot pockets in the N- and C-terminal EF-hand motifs[145].

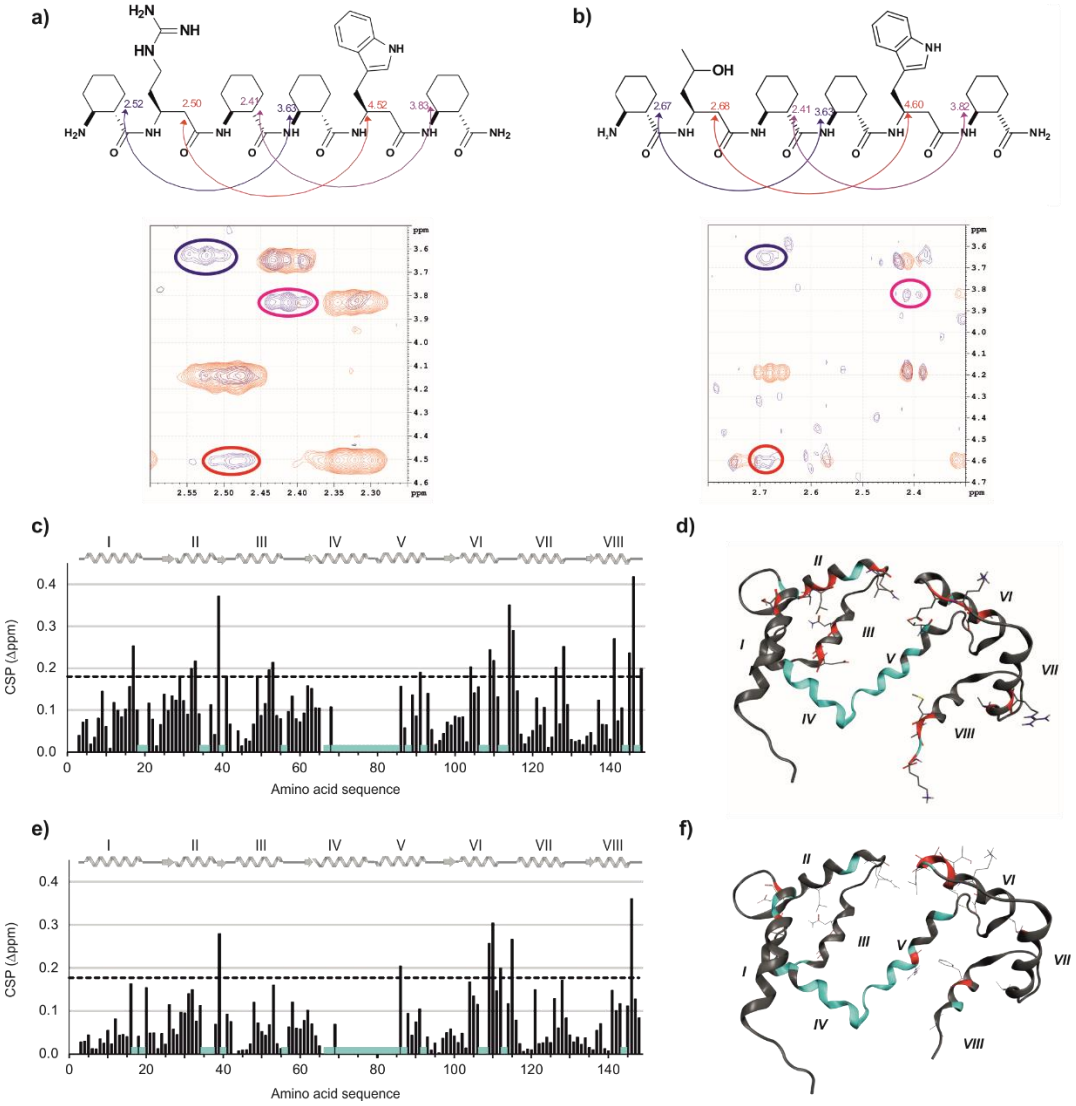

Figure 19. Results of the NMR spectroscopic investigations of foldameric fragments. Tr-NOE interactions showing the helicity of the CaM-bound compounds **a) RW** and **b) TW**; overlaid TOCSY (red) and NOESY spectra acquired with a mixing time of 150 ms (blue). The cross-peaks in the 2D NOESY spectra suggest 14-helix structure of the bound peptides. **c)** CSP of CaM in the presence of **LW** equivalents of 2. Residues with extreme resonance broadening (complete disappearance) are marked with a cyan line. The CSP values were calculated using the formula $[(\Delta\delta(^{1}H))^2 + 0.14 \times (\Delta\delta(^{15}N))^2]^{1/2}$. Dashed lines indicate the mean+standard deviation of the CSP values for the individual titrations, which are used as threshold. **d)** Residues with CSPs above the threshold (red) and the highest resonance broadening (cyan) mapped to the ribbon representation of CaM (PDB code: 2K0E[146]), **e)** and **f)** CSPs

of CaM in the presence of **RW** equivalents of 3; residues with CSPs above the threshold (red) and the highest resonance broadening (cyan) mapped to the ribbon representation of CaM.

4.2.4. Affinity enhancement with dynamic combinatorial chemistry

Twelve different hits were subjected to a target-templated DCL experiment. Three members of each sublibrary were re-synthesized with Gly-Gly-Cys at the C-terminals to prepare DCL through thiol–disulfide exchange reaction[147]. The initial concentartion of each library member was 10 μM in glutathion redox buffer, and the product distributions were analyzed by HPLC-MS in the presence of different protein template concentrations (1, 6, and 30 μM). The reaction mixture reached the thermodynamic equilibrium after 96 hours of incubation: the composition of the solution did not change any more and the same product distribution was obtained from different starting mixture compositions (Figure 20).

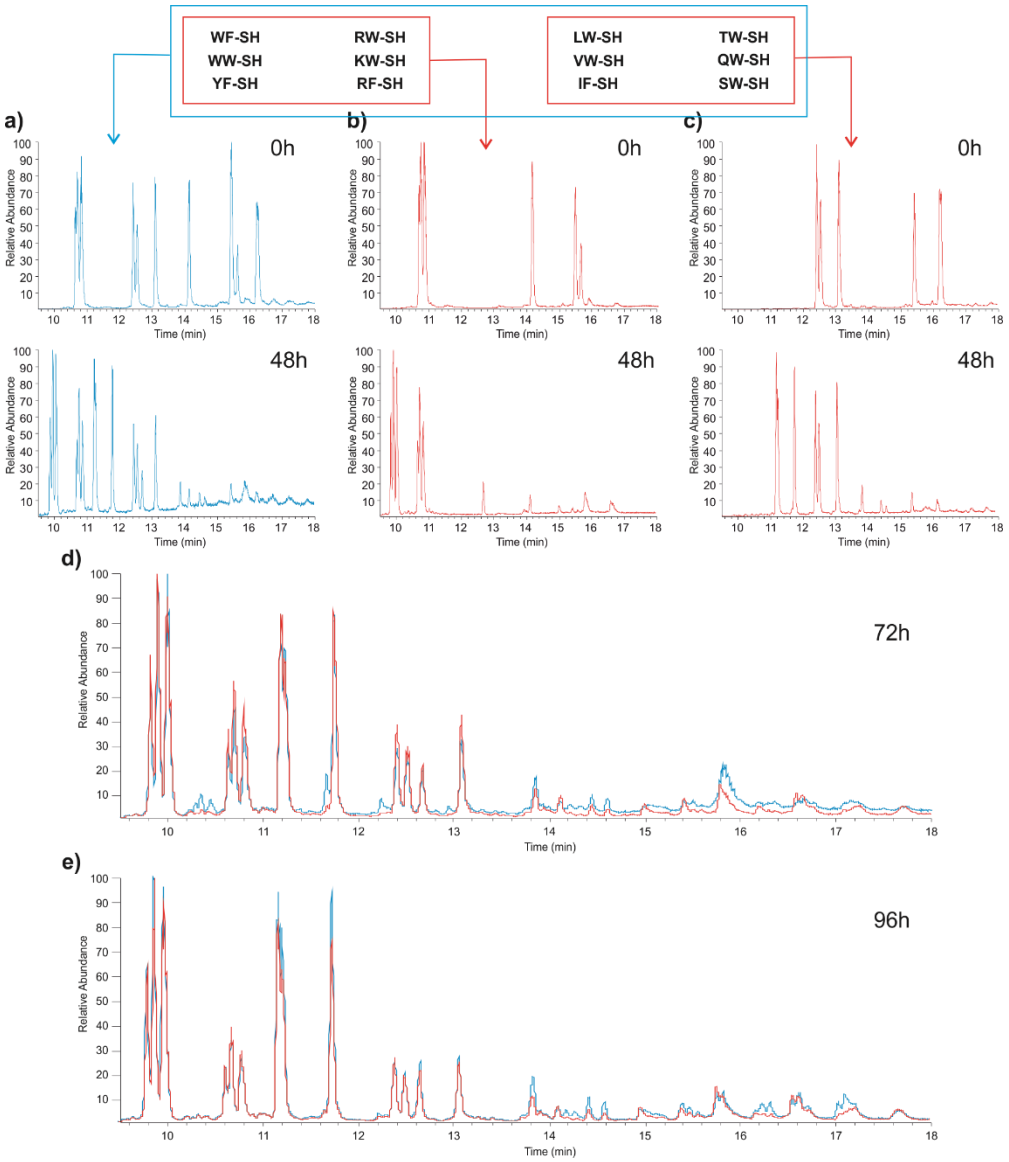

Figure 20. Assessing thermodynamic equilibrium. Total ion chromatograms for DCLs with different mixture compositions at 0 h and pre-equilibrated at 48 h: **a)** library containing all twelve bulding blocks at 10 µM, **b)** and **c)** libraries containing components in the two separate red boxes above. The pre-equilibrated mixtures **b)** and **c)** were pooled after 48 h and the product composition was analyzed after 72 h (**d**) and 96 h (**e**). The final product distribution was compared with the total DCL (blue). After 96 h, only slight differences could be detected between the pooled sample (red) and the control sample (blue). This showed that thermodynamic equilibrium has been reached after 96 h independent of the starting conditions.

Through quantitative evaluation of the HPLC-MS total ion chromatograms, 102 compounds were identified, and the amplification factor was defined for each component by compairing the amount of product in the presence of CaM with that in the control sample (Figure 21). A four-fold increase in the maximum amplification was found as we increased the template concentration from 1 to 30 µM. However, in line with the literature[148], better selectivity was

obtained by keeping the building block to template ratio at high level. From the amplification data thus acquired, it is clear that hydrophobic/aromatic side chains are necessary but not sufficient for high-affinity binding, because under all three conditions dimers with at least one basic side chain are amplified. Interestingly, the homodimers of the best binder fragments (e.g., **WF-SS-WF**) were not amplified despite the quasi-equivalent binding sites on the protein. This, however, may not be surprising since, in the presence of a large excess of template, heterodimers can easily suppress better binder homodimers[148]. Nevertheless, it was found even at 1 μM CaM pointing to an emergent feature originating from the system chemistry approach.

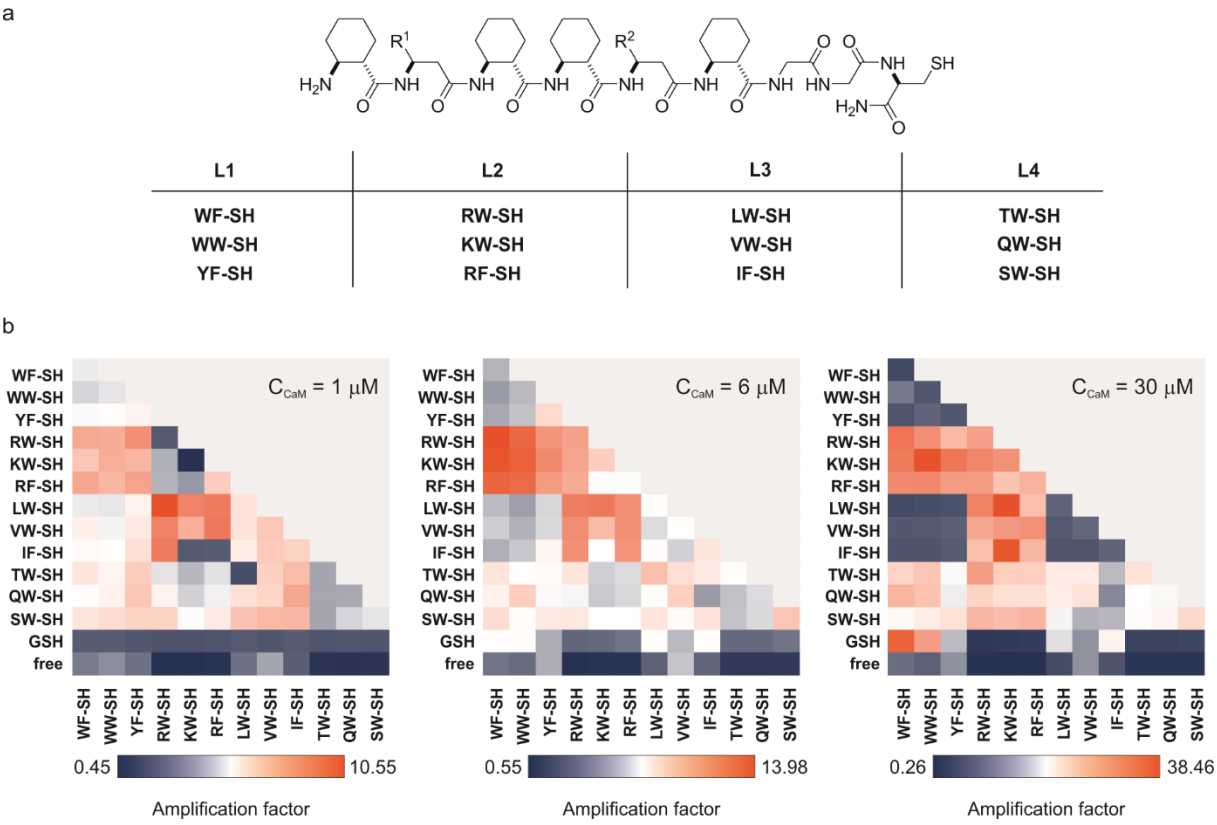

Figure 21. General structural formula and the list of the DCL building blocks (**a**) and **b)** results of the DCL experiments at three different CaM concentrations. The amplification factor was defined as the ratio of the AUCs in the presence of template and in the control sample without the protein. Color scales from blue to red indicate the lowest to highest amplification factor, respectively. „GSH" refers to glutathione adducts and „free" labeled line shows the amplification of a given monomeric building block.

4.2.5. Characterization of the interaction between CaM and the high-affinity ligand

Heterodimer **LW-SS-RW** composed of **LW** and **RW** fragments showed the highest amplification under the most selective experimental conditions; therefore, this was selected as the best ligand. To improve the synthetic efficiency and stability in water, the disulfide bond was replaced by a thioether linkage resulting in **LW-S-RW** (Figure 22a). A two-stage high-

affinity interaction was found between CaM an **LW-S-RW** (Figure 22c) by ITC. The first binding step displayed a K_D of 1.54±0.16 nM with n = 1.04, which is two orders of magnitude lower than that of the monomers.

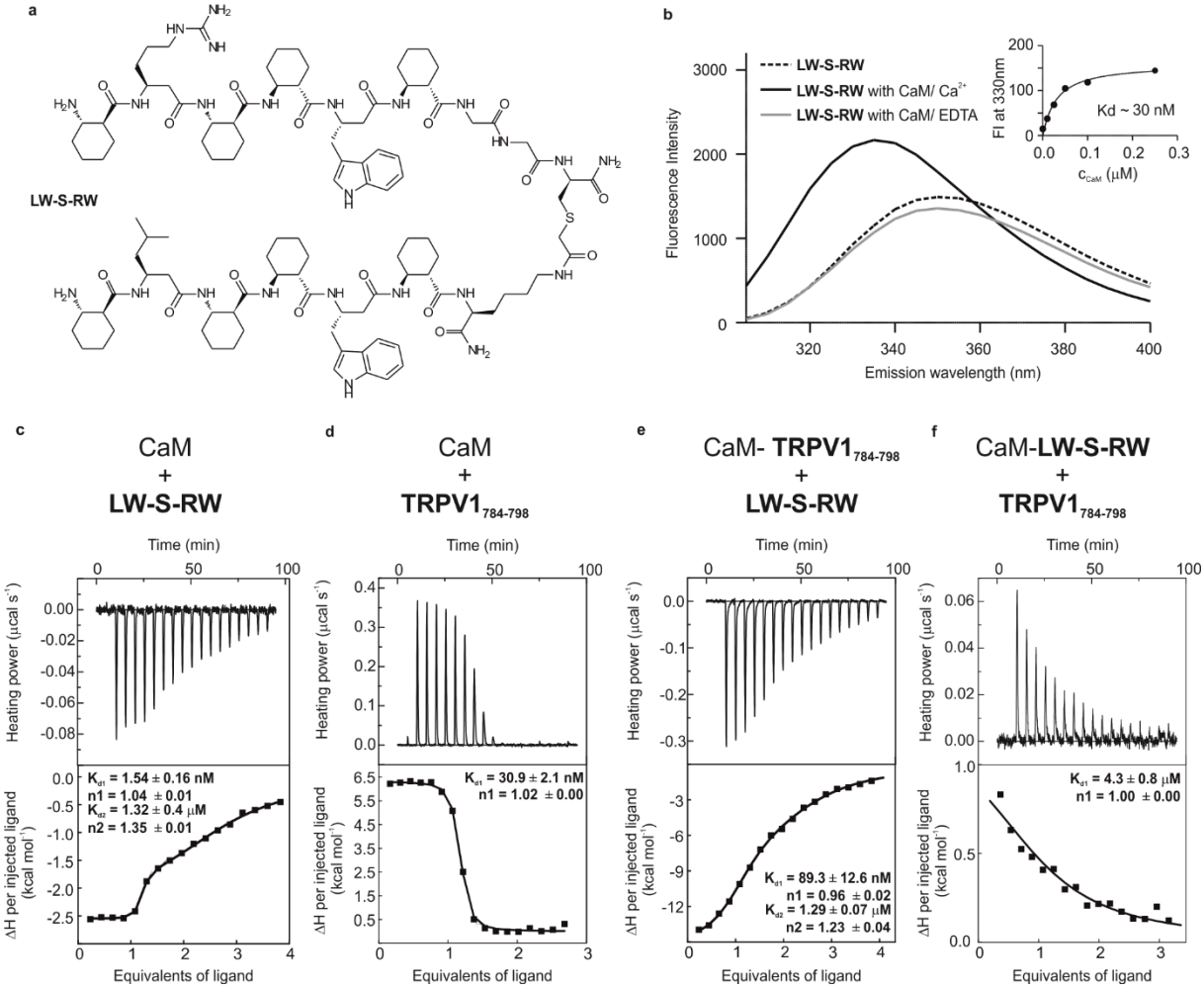

Figure 22. Structure of **LW-S-RW** and characterization of its interaction with CaM. **b**) Trp fluorescence titration experiment, **c**) ITC titration of CaM with **LW-S-RW** and **d**) with $TRPV1_{784–798}$; **e**) and **f**) competitive ITC experiments to confirm the inhibitory potential of the foldameric ligand.

The formation of the 1:1 complex confirmed that the separate hot spots on the protein were successfully targeted with the helix dimer. The second lower-affinity step with fractional stoichiometry was detected, which pointed towards the ability to crosslink protein molecules at micromolar concentration. Owing to the Trp content of the **LW-S-RW**, fluorescence titration experiments could be performed, which also showed Ca^{2+}-dependent binding similar to the monomeric fragments. The estimated affinity was 30 nM, which probably represents the average of the mentioned two-step interaction in ITC (Figure 22b). The interaction between CaM and **LW-S-RW** was also investigated by NMR, in which significant decreases in intensity were found in the ^{1}H-NMR methyl region (0.6–1.08 ppm) of the titrated ^{13}C/^{15}N-labeled CaM (Figure 23a). Significant signal broadening and peak disappearing were found in the ^{15}N HSQC

spectrum (Figure 23b), that could be caused by the ligand, which crosslinked the proteins, thereby slowing down the tumbling rate. This finding together with the existence of the second binding stage in ITC confirmed the crosslinked, **LW-S-RW**-induced formation of CaM associates.

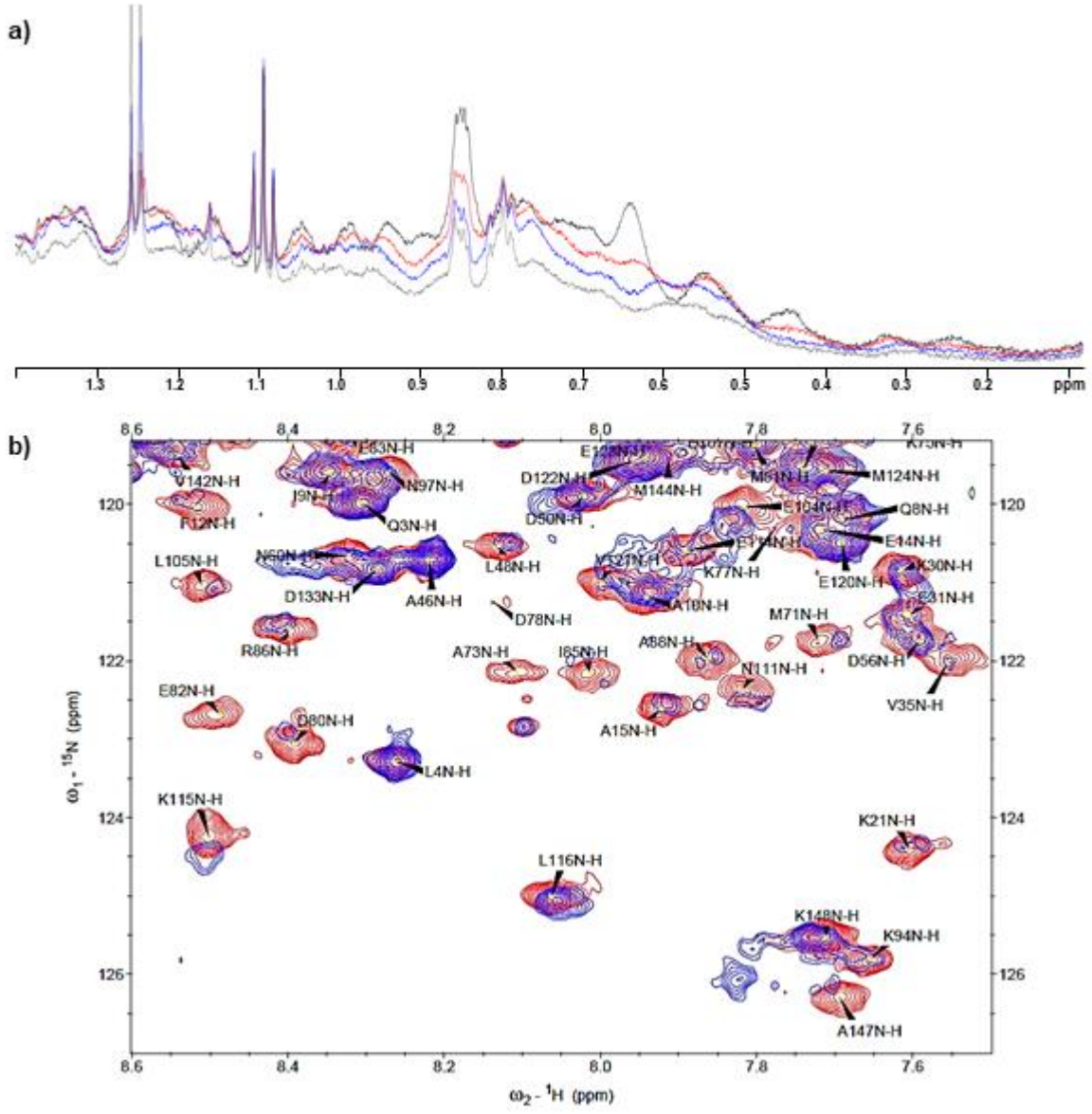

Figure 23. NMR spectroscopic investigation of CaM–**LW-S-RW** interaction. **a)** ^{1}H NMR methyl region of ^{13}C/^{15}N-labeled calmodulin without any ligand (black) and in the presence of 1, 2, and 4 equivalents of **LW-S-RW** (red, blue, and grey, respectively). The corresponding relative integrals between 0.6–1.08 ppm are: 100%, 89%, 77% and 60% for the samples containing 0, 1, 2, and 4 equivalent **LW-S-RW**, respectively; **b)** Selected region for the ^{15}N HSQC spectrum of CaM alone (red) and CaM in the presence of 1 equivalent of **LW-S-RW** (blue).

CaM is a multifunctional Ca^{2+}-binding protein expressed in almost all eukaryotic cells. It has a large number of protein binding partners including interaction with transient receptor potential vanilloid 1 (TRPV1)[149]. This was selected as a model system to test the inhibitory

potential of **LW-S-RW**. In the ITC experiment, the 15-mer peptide fragment $TRPV1_{784–798}$ forms a 1:1 complex with a dissociation constant of 30.9±2.1 nM (Figure 22d). After saturation of the CaM with its native ligand, the complex was titrated with the foldamer and an increased apparent K_D was found for the first binding step (Figure 22e). If the CaM was first saturated with **LW-S-RW** and titrated with $TRPV1_{784–798}$, the apparent affinity increased to the micromolar range (Figure 22f). These competitive ITC experiments confirmed that the foldameric ligand can compete with a native ligand, and it can successfully block their interaction

5. Conclusions

Prior works have reported the effectiveness of foldamers in molecular recognition, but in contrast to top-down approaches, bottom-up strategies are not frequently used for development of foldameric PPI inhibitors. In the present study, *de novo* bottom-up developments of high-affinity foldameric ligands were carried out against difficult protein targets.

Selective recognition of an oligomeric β-amyloid was achieved by the presentation of multiple copies of β-peptides designed as complementary binding surfaces to amyloid KLVFFAE motif. As a result of structural optimization, a tetravalent conjugate was synthesized using oligo-L-lysine dendron as a scaffold, which ensured low nanomolar binding affinity towards Aβ. A foldamer-based ELISA assay was designed using the foldamer-dendron conjugate as a capture element. After detailed optimization, a highly-sensitive affinity assay was developed with 5 pM as the limit of detection, which is comparable to purely antibody-based detection methods. Our test is capable of monitoring the aggregation state of amyloid since it is selective to Aβ surface patterns, transiently present during the ongoing aggregation process. To the best of our knowledge, this is the first application of foldameric sequences in a biochemical assay.

Simultaneous targeting of two separate hot spots of protein was utilized through systematic testing of a foldameric fragment library. A diverse 256-membered foldamer fragment library was designed and synthesized, and its binding affinity to CaM as model protein was tested in pulldown assays. The number of enriched fragments and the side-chain chemistry were in line with the pleiotropic behavior of the protein and the common structural motifs of its binding partners. This confirmed the ability of foldamer library to mimic protein surface patches. Selected foldameric fragments could simultaneously recognize the separate hot spots by forming 2:1 complexes with CaM. Their low micromolar binding affinities displayed the maximum achievable affinity, through projecting only two interacting side chains towards the

surface. With ^{15}N-HSQC titration, residues, known to be key residues in the CaM–protein contacts, were identified. For the first time, dynamic combinatorial chemistry was used for development of foldameric ligands that recognized discontinuous hot spots. Considering the guidelines of DCL formation, an amplification study was carried out, that resulted in a heterodimeric foldamer ligand with a significantly improved binding affinity towards CaM. The existence of the 1:1 complex in ITC revealed the simultaneous recognition of the hot spots by a single foldameric ligand. Moreover, the dimer proved to be an effective inhibitor of CaM–vanilloid receptor interaction.

This study presented two different bottom-up approaches for efficient optimization of foldameric ligands. First, following the steps of the fragment-based drug design, functional mimetic of the molecular recognition properties of an antibody was prepared. The specific arrangement of multiple copies of epitope mimetics made the foldameric conjugate applicable to be utilized in a sensitive biochemical assay. In the second part of this work, a feasible synthetic strategy was elaborated in detail leading to a high-affinity foldameric PPI inhibitor by combining HTS of local surface mimetics and their dynamic covalent coupling.

6. Summary

1. Utilizing the interaction between a previously studied antibody mimetic tetravalent foldamer–dendrimer conjugate and β-amyloid, a sandwich type analytical biochemistry assay was designed for detection and quantification of aggregated β-amyloid species in low nanomolar concentration.
   1.1. 16 different conjugates were designed and produced by convergent synthesis to study the relationship between the structure of the foldameric ligand and binding affinity to β-amyloid. A rising trend in efficiency was observed by increasing the number of arms of the conjugate, but the low nanomolar affinity could not be further enhanced by introducing an octavalent template instead of a tetravalent.
   1.2. Linking the 14-helix foldamers to a tetravalent oligo-L-lysine dendron scaffold resulted in a branched conjugate that binds to β-amyloid with high affinity similar to foldamer-dendrimer, but it had more favorable properties for immobilization. Foldameric fragments on an oligo-L-lysine dendron were successfully used as capture elements in a sandwich ELISA experiment.
   1.3. The optimized assay was able to distinguish between β-amyloid monomers and associated forms with high selectivity toward soluble β-amyloid oligomer, a potential biomarker in early diagnosis of Alzheimer's disease. A detection limit of 5 pM was achieved, which indicated the high sensitivity of the newly developed ELISA test.
2. A modular bottom-up approach was used to create foldameric protein–protein interaction inhibitor for separate hot spots.
   2.1. A 256-membered foldamer library was designed and synthesized containing diverse surface patch mimetic 14-helix fragments. The affinity of the library members toward the model protein calmodulin with separate hot spots was tested in a pulldown assay, and hits having a high propensity to form a complex with the protein were determined.
   2.2. Binding efficiencies of the four selected hits were quantified by two parallel experiments – ITC and fluorescence titration – and interactions were found in the low micromolar to submicromolar range.
   2.3. The best 12 fragments of the library were synthesized individually with free thiol functionality and a dynamic combinatorial library was generated in a glutathione redox buffer using calmodulin as template. Under this experimental condition, the best binding ligand was the thermodynamically most favored species, because the selection of the products is based on their position in the free energy landscape. Product

distribution of the 102-membered DCLs was analyzed and the most amplified dimeric helix considered to be the best ligand for calmodulin was selected for further characterization.

2.4. The best ligand was re-synthesized via linking the fragments in appropiate orientation by the thioether linkage. It showed dissociation constants two orders of magnitude lower than those of the monomeric fragments. Competitive experiments confirmed that the foldameric ligand bound to the same binding site as the native ligand (C-terminal of the vanilloid receptor) and the foldamer can function as a protein–protein interaction inhibitor.

7. Acknowledgements

Firstly, I would like to express my sincere gratitude to my supervisor Prof. Tamás Martinek for the continuous support of my Ph.D. study and related research, for his motivation and immense knowledge. His guidance helped me in all the time of research and writing of this thesis.

My sincere thanks also go to Dr. Lívia Fülöp, and her research group in the Department of Medical Chemistry, especially to Dr. Ildikó Schuster for performing in vitro binding assays and to Dr. Zsolt Bozsó for the stimulating discussions about peptide synthesis methods.

I owe my special thanks to Dr. Zsófia Hegedüs; without her precious support it would not be possible to conduct this research.

I am also grateful to Dr. Edit Wéber for performing the NMR measurements and for her constructive comments.

I would like to thank Prof. Dr. Ferenc Fülöp for providing me the possibility to carry out part of my work at the Institute of Pharmaceutical Chemistry.

I owe my thanks to all my colleagues for their help and useful advice and for all the fun we have had in the last couple of years.

Last but not least, I would like to thank my family and friends for supporting me spiritually during my Ph.D. studies.

8. References

[1] E. Persch, O. Dumele, F. Diederich, *Angewandte Chemie International Edition* **2015**, *54*, 3290-3327.

[2] J.-M. Lehn, *Supramolecular chemistry, Vol. 1*, Vch, Weinheim Germany, **1995**.

[3] J. Rebek, *Proceedings of the National Academy of Sciences of the United States of America* **2009**, *106*, 10423-10424.

[4] M. C. Smith, J. E. Gestwicki, *Expert reviews in molecular medicine* **2012**, *14*, 1-24.

[5] C. A. Hunter, *Angewandte Chemie International Edition* **2004**, *43*, 5310-5324.

[6] D. E. Scott, A. R. Bayly, C. Abell, J. Skidmore, *Nature Reviews Drug Discovery* **2016**, *15*, 533-550.

[7] N. Tsomaia, *Eur J Med Chem* **2015**, *94*, 459-470.

[8] A. A. Bogan, K. S. Thorn, *J Mol Biol* **1998**, *280*, 1-9.

[9] S. Jones, J. M. Thornton, *J Mol Biol* **1997**, *272*, 121-132.

[10] I. S. Moreira, P. A. Fernandes, M. J. Ramos, *Proteins: Structure, Function, and Bioinformatics* **2007**, *68*, 803-812.

[11] N. London, B. Raveh, O. Schueler-Furman, *Curr Opin Chem Biol* **2013**, *17*, 952-959.

[12] M. Gao, K. Cheng, H. J. P. S. Yin, *Biopolymers* **2015**, *104*, 310-316.

[13] P. Wójcik, Ł. Berlicki, *Bioorg Med Chem Lett.* **2016**, *26*, 707-713.

[14] C. M. Goodman, S. Choi, S. Shandler, W. F. DeGrado, *Nature Chemical Biology* **2007**, *3*, 252-262.

[15] H. M. Werner, W. S. Horne, *Curr Opin Chem Biol* **2015**, *28*, 75-82.

[16] C. Cabrele, T. s. A. Martinek, O. Reiser, Ł. Berlicki, *J Med Chem* **2014**, *57*, 9718-9739.

[17] I. M. Mándity, E. Wéber, T. A. Martinek, G. Olajos, G. K. Tóth, E. Vass, F. Fülöp, *Angewandte Chemie International Edition* **2009**, *48*, 2171-2175.

[18] L. K. Pilsl, O. Reiser, *Amino acids* **2011**, *41*, 709-718.

[19] R. Maini, S. R. Chowdhury, L. M. Dedkova, B. Roy, S. M. Daskalova, R. Paul, S. Chen, S. M. J. B. Hecht, *Biochemistry* **2015**, *54*, 3694-3706.

[20] I. Benilova, E. Karran, B. De Strooper, *Nature Neuroscience* **2012**, *15*, 349-357.

[21] M. Ahmed, J. Davis, D. Aucoin, T. Sato, S. Ahuja, S. Aimoto, J. I. Elliott, W. E. Van Nostrand, S. O. Smith, *Nature Structural & Molecular Biology* **2010**, *17*, 561-567.

[22] A. R. A. Ladiwala, J. Litt, R. S. Kane, D. S. Aucoin, S. O. Smith, S. Ranjan, J. Davis, W. E. VanNostrand, P. M. Tessier, *J Biol Chem* **2012**, *287*, 24765-24773.

[23] K. E. Marshall, D. M. Vadukul, L. Dahal, A. Theisen, M. W. Fowler, Y. Al-Hilaly, L. Ford, G. Kemenes, I. J. Day, K. Staras, *Sci Rep* **2016**, *6*, 30182-30195.

[24] C. Haass, D. J. Selkoe, *Nature Reviews Molecular Cell Biology* **2007**, *8*, 101-112.

[25] D. J. Selkoe, J. Hardy, *EMBO molecular medicine* **2016**, *8*, 595-608.

[26] A. Crivici, M. Ikura, *Annual review of biophysics and biomolecular structure* **1995**, *24*, 85-116.

[27] K. P. Hoeflich, M. Ikura, *Cell* **2002**, *108*, 739-742.

[28] P. T. Corbett, J. Leclaire, L. Vial, K. R. West, J.-L. Wietor, J. K. Sanders, S. Otto, *Chemical reviews* **2006**, *106*, 3652-3711.

[29] U. Stelzl, U. Worm, M. Lalowski, C. Haenig, F. H. Brembeck, H. Goehler, M. Stroedicke, M. Zenkner, A. Schoenherr, S. Koeppen, J. Timm, S. Mintzlaff, C. Abraham, N. Bock, S. Kietzmann, A. Goedde, E. Toksoz, A. Droege, S. Krobitsch, B. Korn, W. Birchmeier, H. Lehrach, E. E. Wanker, *Cell* **2005**, *122*, 957-968.

[30] G. Kar, A. Gursoy, O. Keskin, *PLoS Comput Biol* **2009**, *5*, 1-18.

[31] G. Kar, G. Kuzu, O. Keskin, A. Gursoy, *Current pharmaceutical design* **2012**, *18*, 4697-4705.

[32] J. W. Checco, S. H. Gellman, *Curr Opin Struct Biol* **2016**, *39*, 96-105.

[33] O. Keskin, A. Gursoy, B. Ma, R. Nussinov, *Chemical reviews* **2008**, *108*, 1225-1244.
[34] L. Young, R. Jernigan, D. Covell, *Protein Science* **1994**, *3*, 717-729.
[35] C. J. Camacho, Z. Weng, S. Vajda, C. DeLisi, *Biophys J* **1999**, *76*, 1166-1178.
[36] D. Xu, C.-J. Tsai, R. Nussinov, *Protein engineering* **1997**, *10*, 999-1012.
[37] O. Keskin, B. Ma, R. Nussinov, *J Mol Biol* **2005**, *345*, 1281-1294.
[38] P. Chakrabarti, J. Janin, *Proteins* **2002**, *47*, 334-343.
[39] B. Ma, T. Elkayam, H. Wolfson, R. Nussinov, *Proceedings of the National Academy of Sciences of the United States of America* **2003**, *100*, 5772-5777.
[40] J. W. Tilley, L. Chen, D. C. Fry, S. D. Emerson, G. D. Powers, D. Biondi, T. Varnell, R. Trilles, R. Guthrie, F. Mennona, *J Am Chem Soc* **1997**, *119*, 7589-7590.
[41] L. Chen, H. Yin, B. Farooqi, S. Sebti, A. D. Hamilton, J. Chen, *Molecular cancer therapeutics* **2005**, *4*, 1019-1025.
[42] M. Vogler, D. Dinsdale, M. J. Dyer, G. M. J. C. d. Cohen, differentiation, *Cell Death and Differ.* **2009**, *16*, 360-367.
[43] M. R. Arkin, Y. Tang, J. A. Wells, *Chemistry & biology* **2014**, *21*, 1102-1114.
[44] S. J. Buhrlage, C. A. Bates, S. P. Rowe, A. R. Minter, B. B. Brennan, C. Y. Majmudar, D. E. Wemmer, H. Al-Hashimi, A. K. Mapp, *ACS Chem Biol* **2009**, *4*, 335-344.
[45] L. von Kleist, W. Stahlschmidt, H. Bulut, K. Gromova, D. Puchkov, M. J. Robertson, K. A. MacGregor, N. Tomilin, A. Pechstein, N. Chau, *Cell* **2011**, *146*, 471-484.
[46] T. Maurer, L. S. Garrenton, A. Oh, K. Pitts, D. J. Anderson, N. J. Skelton, B. P. Fauber, B. Pan, S. Malek, D. Stokoe, *Proceedings of the National Academy of Sciences of the United States of America* **2012**, *109*, 5299-5304.
[47] J. A. Wells, C. L. McClendon, *Nature* **2007**, *450*, 1001-1009.
[48] A. J. Wilson, *Chemical Society Reviews* **2009**, *38*, 3289-3300.
[49] X. Yu, Y.-P. Yang, E. Dikici, S. K. Deo, S. Daunert, *Annual Review of Analytical Chemistry* **2017**, *10*, 293-320.
[50] A. R. Baloch, A. W. Baloch, B. J. Sutton, X. Zhang, *Critical reviews in biotechnology* **2016**, *36*, 268-275.
[51] C. I. Justino, A. C. Duarte, T. A. Rocha-Santos, *TrAC Trends in Analytical Chemistry* **2015**, *65*, 73-82.
[52] X. Wu, J. Chen, M. Wu, J. X. Zhao, *Theranostics* **2015**, *5*, 322-344.
[53] K. Škrlec, B. Štrukelj, A. Berlec, *Trends in Biotechnology* **2015**, *33*, 408-418.
[54] S. H. Hewitt, A. J. Wilson, *Chem Commun (Camb)* **2016**, *52*, 9745-9756.
[55] S. B. Nimse, T. Kim, *Chemical Society Reviews* **2013**, *42*, 366-386.
[56] D. Aviezer, S. Cotton, M. David, A. Segev, N. Khaselev, N. Galili, Z. Gross, A. Yayon, *Cancer Research* **2000**, *60*, 2973-2980.
[57] O. Hayashida, N. Ogawa, M. Uchiyama, *J Am Chem Soc* **2007**, *129*, 13698-13705.
[58] H. Zhou, L. Liu, J. Huang, D. Bernard, H. Karatas, A. Navarro, M. Lei, S. Wang, *J Med Chem* **2013**, *56*, 1113-1123.
[59] L. D. Walensky, G. H. Bird, *J Med Chem* **2014**, *57*, 6275-6288.
[60] G. L. Verdine, G. J. Hilinski, *Methods Enzymol* **2012**, *503*, 3-33.
[61] S. Baek, P. S. Kutchukian, G. L. Verdine, R. Huber, T. A. Holak, K. W. Lee, G. M. Popowicz, *J Am Chem Soc* **2011**, *134*, 103-106.
[62] A. Patgiri, A. L. Jochim, P. S. Arora, *Acc Chem Res* **2008**, *41*, 1289-1300.
[63] R. N. Chapman, G. Dimartino, P. S. Arora, *J Am Chem Soc* **2004**, *126*, 12252-12253.
[64] J. A. Robinson, *Acc Chem Res* **2008**, *41*, 1278-1288.
[65] F. Zoller, A. Markert, P. Barthe, W. Zhao, W. Weichert, V. Askoxylakis, A. Altmann, W. Mier, U. Haberkorn, *Angewandte Chemie International Edition* **2012**, *51*, 13136-13139.

[66] B. D. Welch, A. P. VanDemark, A. Heroux, C. P. Hill, M. S. Kay, *Proceedings of the National Academy of Sciences of the United States of America* **2007**, *104*, 16828-16833.
[67] M. Liu, C. Li, M. Pazgier, C. Li, Y. Mao, Y. Lv, B. Gu, G. Wei, W. Yuan, C. Zhan, *Proceedings of the National Academy of Sciences of the United States of America* **2010**, *107*, 14321-14326.
[68] C. Li, M. Pazgier, J. Li, C. Li, M. Liu, G. Zou, Z. Li, J. Chen, S. G. Tarasov, W.-Y. Lu, *J Biol Chem* **2010**, *285*, 19572-19581.
[69] S. A. Fowler, H. E. Blackwell, *Organic & biomolecular chemistry* **2009**, *7*, 1508-1524.
[70] J. S. Laursen, J. Engel-Andreasen, C. A. Olsen, *Acc Chem Res* **2015**, *48*, 2696-2704.
[71] J. Sun, R. N. Zuckermann, *ACS Nano* **2013**, *7*, 4715-4732.
[72] S. H. Gellman, *Acc Chem Res* **1998**, *31*, 173-180.
[73] S. Hecht, I. Huc, *Foldamers: structure, properties and applications*, John Wiley & Sons, **2007**.
[74] J. Frackenpohl, P. I. Arvidsson, J. V. Schreiber, D. Seebach, *ChemBioChem* **2001**, *2*, 445-455.
[75] J. D. Sadowsky, J. K. Murray, Y. Tomita, S. H. Gellman, *ChemBioChem* **2007**, *8*, 903-916.
[76] Z. Hegedüs, T. A. Martinek, in *Comprehensive Supramolecular Chemistry II*, **2017**, pp. 511-537.
[77] E. Juaristi, V. A. Soloshonok, *Enantioselective synthesis of beta-amino acids*, John Wiley & Sons, **2005**.
[78] W. Kirmse, *Eur J Org Chem* **2002**, *2002*, 2193-2256.
[79] D. Seebach, J. Gardiner, *Acc Chem Res* **2008**, *41*, 1366-1375.
[80] G. Lelais, P. Micuch, D. Josien-Lefebvre, F. Rossi, D. Seebach, *Helvetica Chimica Acta* **2004**, *87*, 3131-3159.
[81] F. Fulop, T. A. Martinek, G. K. Toth, *Chemical Society Reviews* **2006**, *35*, 323-334.
[82] W. S. Horne, L. M. Johnson, T. J. Ketas, P. J. Klasse, M. Lu, J. P. Moore, S. H. Gellman, *Proceedings of the National Academy of Sciences of the United States of America* **2009**, *106*, 14751-14756.
[83] T. A. Martinek, F. Fülöp, *Chemical Society Reviews* **2012**, *41*, 687-702.
[84] É. Szolnoki, A. Hetényi, T. A. Martinek, Z. Szakonyi, F. Fülöp, *Organic & biomolecular chemistry* **2012**, *10*, 255-259.
[85] É. Szolnoki, A. Hetényi, I. M. Mándity, F. Fülöp, T. A. Martinek, *Eur J Org Chem* **2013**, *2013*, 3555-3559.
[86] Ł. Berlicki, L. Pilsl, E. Wéber, I. M. Mándity, C. Cabrele, T. A. Martinek, F. Fülöp, O. Reiser, *Angewandte Chemie International Edition* **2012**, *51*, 2208-2212.
[87] W. S. Horne, S. H. Gellman, *Acc Chem Res* **2008**, *41*, 1399-1408.
[88] J. D. Sadowsky, M. A. Schmitt, H.-S. Lee, N. Umezawa, S. Wang, Y. Tomita, S. H. Gellman, *J Am Chem Soc* **2005**, *127*, 11966-11968.
[89] J. A. Kritzer, J. D. Lear, M. E. Hodsdon, A. Schepartz, *J Am Chem Soc* **2004**, *126*, 9468-9469.
[90] E. A. Harker, A. Schepartz, *ChemBioChem* **2009**, *10*, 990-993.
[91] H. S. Haase, K. J. Peterson-Kaufman, S. K. Lan Levengood, J. W. Checco, W. L. Murphy, S. H. Gellman, *J Am Chem Soc* **2012**, *134*, 7652-7655.
[92] K. Gademann, M. Ernst, D. Hoyer, D. Seebach, *Angewandte Chemie International Edition* **1999**, *38*, 1223-1226.
[93] R. W. Cheloha, A. Maeda, T. Dean, T. J. Gardella, S. H. Gellman, *Nature Biotechnology* **2014**, *32*, 653-655.
[94] L. M. Johnson, S. Barrick, M. V. Hager, A. McFedries, E. A. Homan, M. E. Rabaglia, M. P. Keller, A. D. Attie, A. Saghatelian, A. Bisello, *J Am Chem Soc* **2014**, *136*, 12848-12851.
[95] W. S. Horne, M. D. Boersma, M. A. Windsor, S. H. Gellman, *Angewandte Chemie International Edition* **2008**, *47*, 2853-2856.
[96] D. E. Scott, A. G. Coyne, S. A. Hudson, C. Abell, *Biochemistry* **2012**, *51*, 4990-5003.

[97] M. Baker, *Vol. 12*, Nature Reviews Drug Discovery, **2012**, pp. 5-7.
[98] L. Fülöp, I. M. Mándity, G. Juhász, V. Szegedi, A. Hetényi, E. Wéber, Z. Bozsó, D. Simon, M. Benkő, Z. Király, *PLoS One* **2012**, *7*, 1-17.
[99] C. Guarise, S. Shinde, K. Kibler, G. Ghirlanda, L. J. Prins, P. Scrimin, *Tetrahedron* **2012**, *68*, 4346-4352.
[100] A. M. Davis, A. T. Plowright, E. Valeur, *Nature Reviews Drug Discovery* **2017**, *16*, 681-698.
[101] O. Ramström, J.-M. Lehn, *Nature Reviews Drug Discovery* **2002**, *1*, 26-36.
[102] L. Milanesi, C. A. Hunter, S. E. Sedelnikova, J. P. Waltho, *Chemistry-A European Journal* **2006**, *12*, 1081-1087.
[103] A. Herrmann, *Chemical Society Reviews* **2014**, *43*, 1899-1933.
[104] J. N. Reek, S. Otto, *Dynamic combinatorial chemistry*, John Wiley & Sons, **2010**.
[105] I. Saur, K. Severin, *Chemical Communications* **2005**, 1471-1473.
[106] P. T. Corbett, S. Otto, J. K. Sanders, *Chemistry-A European Journal* **2004**, *10*, 3139-3143.
[107] P. T. Corbett, J. K. Sanders, S. Otto, *Angewandte Chemie International Edition* **2007**, *46*, 8858-8861.
[108] C. A. Ross, M. A. Poirier, *Nature Medicine* **2004**, *10*, 10-17.
[109] J. Hardy, D. J. Selkoe, *Science* **2002**, *297*, 353-356.
[110] G. Bitan, M. D. Kirkitadze, A. Lomakin, S. S. Vollers, G. B. Benedek, D. B. Teplow, *Proceedings of the National Academy of Sciences of the United States of America* **2003**, *100*, 330-335.
[111] M. L. Giuffrida, F. Caraci, B. Pignataro, S. Cataldo, P. De Bona, V. Bruno, G. Molinaro, G. Pappalardo, A. Messina, A. Palmigiano, D. Garozzo, F. Nicoletti, E. Rizzarelli, A. Copani, *J Neurosci* **2009**, *29*, 10582-10587.
[112] K. Blennow, N. Mattsson, M. Schöll, O. Hansson, H. Zetterberg, *Trends in Pharmacological Sciences* **2015**, *36*, 297-309.
[113] J. X. Lu, W. Qiang, W. M. Yau, C. D. Schwieters, S. C. Meredith, R. Tycko, *Cell* **2013**, *154*, 1257-1268.
[114] A. Laganowsky, C. Liu, M. R. Sawaya, J. P. Whitelegge, J. Park, M. Zhao, A. Pensalfini, A. B. Soriaga, M. Landau, P. K. Teng, D. Cascio, C. Glabe, D. Eisenberg, *Science* **2012**, *335*, 1228-1231.
[115] I. A. Mastrangelo, M. Ahmed, T. Sato, W. Liu, C. Wang, P. Hough, S. O. Smith, *J Mol Biol* **2006**, *358*, 106-119.
[116] Z. Fu, D. Aucoin, M. Ahmed, M. Ziliox, W. E. Van Nostrand, S. O. Smith, *Biochemistry* **2014**, *53*, 7893-7903.
[117] M. T. Colvin, R. Silvers, Q. Z. Ni, T. V. Can, I. Sergeyev, M. Rosay, K. J. Donovan, B. Michael, J. Wall, S. Linse, R. G. Griffin, *J Am Chem Soc* **2016**, *138*, 9663-9674.
[118] M. J. Hajipour, M. R. Santoso, F. Rezaee, H. Aghaverdi, M. Mahmoudi, G. Perry, *Trends in Biotechnology* **2017**, *35*, 937-953.
[119] K. A. Johnson, N. C. Fox, R. A. Sperling, W. E. Klunk, *Cold Spring Harbor perspectives in medicine* **2012**, *2*, 1-13.
[120] H. Englund, D. Sehlin, A. S. Johansson, L. N. Nilsson, P. Gellerfors, S. Paulie, L. Lannfelt, F. E. Pettersson, *J Neurochem* **2007**, *103*, 334-345.
[121] H. Fukumoto, T. Tokuda, T. Kasai, N. Ishigami, H. Hidaka, M. Kondo, D. Allsop, M. Nakagawa, *FASEB J* **2010**, *24*, 2716-2726.
[122] S. A. Funke, E. Birkmann, F. Henke, P. Gortz, C. Lange-Asschenfeldt, D. Riesner, D. Willbold, *Biochem Biophys Res Commun* **2007**, *364*, 902-907.
[123] S. A. Funke, E. Birkmann, F. Henke, P. Gortz, C. Lange-Asschenfeldt, D. Riesner, D. Willbold, *Rejuvenation Res* **2008**, *11*, 315-318.

[124] C. M. Gao, A. Y. Yam, X. Wang, E. Magdangal, C. Salisbury, D. Peretz, R. N. Zuckermann, M. D. Connolly, O. Hansson, L. Minthon, H. Zetterberg, K. Blennow, J. P. Fedynyshyn, S. Allauzen, *PLoS One* **2010**, *5*, 1-7.
[125] D. G. Georganopoulou, L. Chang, J.-M. Nam, C. S. Thaxton, E. J. Mufson, W. L. Klein, C. A. Mirkin, *Proceedings of the National Academy of Sciences of the United States of America* **2005**, *102*, 2273-2276.
[126] A. J. Haes, L. Chang, W. L. Klein, R. P. Van Duyne, *J Am Chem Soc* **2005**, *127*, 2264-2271.
[127] M. Kamali-Moghaddam, F. E. Pettersson, D. Wu, H. Englund, S. Darmanis, A. Lord, G. Tavoosidana, D. Sehlin, S. Gustafsdottir, L. N. Nilsson, *BMC neuroscience* **2010**, *11*, 124-131.
[128] L. Liu, N. Xia, M. Jiang, N. Huang, S. Guo, S. Li, S. Zhang, *Journal of Electroanalytical Chemistry* **2015**, *754*, 40-45.
[129] A. N. Santos, S. Torkler, D. Nowak, C. Schlittig, M. Goerdes, T. Lauber, L. Trischmann, M. Schaupp, M. Penz, F.-W. Tiller, *Journal of Alzheimer's Disease* **2007**, *11*, 117-125.
[130] A. N. Santos, M. Ewers, L. Minthon, A. Simm, R.-E. Silber, K. Blennow, D. Prvulovic, O. Hansson, H. Hampel, *Journal of Alzheimer's disease* **2012**, *29*, 171-176.
[131] A. J. Veloso, A. M. Chow, H. V. Ganesh, N. Li, D. Dhar, D. C. Wu, S. Mikhaylichenko, I. R. Brown, K. Kerman, *Anal Chem* **2014**, *86*, 4901-4909.
[132] Z. Bozso, B. Penke, D. Simon, I. Laczkó, G. Juhász, V. Szegedi, Á. Kasza, K. Soós, A. Hetényi, E. Wéber, *Peptides* **2010**, *31*, 248-256.
[133] S. N. Thomas, D. Cripps, A. J. Yang, in *Neuroproteomics*, Springer, **2009**, pp. 109-121.
[134] S. Hunter, C. Brayne, *Journal of negative results in biomedicine* **2017**, *16*, 1-8.
[135] W. Xia, T. Yang, I. M. Smith, Y. Shen, D. M. Walsh, D. J. Selkoe, *Archives of neurology* **2009**, *66*, 190-199.
[136] R. P. Haugland, W. W. You, in *The Protein Protocols Handbook*, Springer, **2002**, pp. 355-363.
[137] L. Li, I. Vorobyov, T. W. Allen, *The Journal of Physical Chemistry B* **2013**, *117*, 11906-11920.
[138] N. Carulla, M. Zhou, E. Giralt, C. V. Robinson, C. M. Dobson, *Acc Chem Res* **2010**, *43*, 1072-1079.
[139] H. Tidow, P. Nissen, *Febs Journal* **2013**, *280*, 5551-5565.
[140] J. A. Boutin, I. Gesson, J.-M. Henlin, S. Bertin, P.-H. Lambert, J.-P. Volland, J.-L. Fauchère, *Molecular diversity* **1997**, *3*, 43-60.
[141] J. M. Ostresh, J. H. Winkle, V. T. Hamashin, R. A. Houghten, *Biopolymers: Original Research on Biomolecules* **1994**, *34*, 1681-1689.
[142] J. E. Ladbury, G. Klebe, E. Freire, *Nature Reviews Drug Discovery* **2010**, *9*, 23-27.
[143] T. Yuan, A. M. Weljie, H. J. Vogel, *Biochemistry* **1998**, *37*, 3187-3195.
[144] A. M. Weljie, H. J. Vogel, *Protein engineering* **2000**, *13*, 59-66.
[145] A. Villarroel, M. Taglialatela, G. Bernardo-Seisdedos, A. Alaimo, J. Agirre, A. Alberdi, C. Gomis-Perez, M. V. Soldovieri, P. Ambrosino, C. Malo, *J Mol Biol* **2014**, *426*, 2717-2735.
[146] J. Gsponer, J. Christodoulou, A. Cavalli, J. M. Bui, B. Richter, C. M. Dobson, M. Vendruscolo, *Structure* **2008**, *16*, 736-746.
[147] S. P. Black, J. K. Sanders, A. R. Stefankiewicz, *Chemical Society Reviews* **2014**, *43*, 1861-1872.
[148] P. T. Corbett, J. K. Sanders, S. Otto, *J Am Chem Soc* **2005**, *127*, 9390-9392.
[149] S.-Y. Lau, E. Procko, R. Gaudet, *The Journal of general physiology* **2012**, *140*, 541-555.